

Boundary element strategies and discretized Green's functions:  
applications in composite materials and wave mechanics

by

Lingyun Pan

A dissertation submitted to the graduate faculty  
in partial fulfillment of the requirements for the degree of

DOCTOR OF PHILOSOPHY

Major: Engineering Mechanics

Major Professor: Frank J. Rizzo

Iowa State University

Ames, Iowa

1997

Graduate College  
Iowa State University

This is to certify that the Doctoral dissertation of  
  
Lingyun Pan  
  
has met the dissertation requirements of Iowa State University

---

Major Professor

---

For the Major Program

---

For the Graduate College

## TABLE OF CONTENTS

<b>GENERAL INTRODUCTION</b>	1
BIE/BEM	1
Green's Functions	2
Applications	5
Dissertation Organization	7
References	9
<b>CHAPTER 1. EXACT GREEN'S FUNCTIONS AND THE BOUNDARY ELEMENT METHOD</b>	12
Introduction	12
Exact Green's Functions and the BIE Process	13
Some Approximate Forms and Solution Strategies	16
Numerical Examples	18
An Alternative for Getting Discretized Green's Function from CBIE	19
The Library Idea	22
References	23
<b>CHAPTER 2. BEM ANALYSIS FOR COMPOSITE MATERIALS AND A LIBRARY OF GREEN'S FUNCTIONS</b>	28
Abstract	28
Introduction	29
Method of Analysis	31
BEM Formulation	33
Numerical Examples	37
A Library of Green's Functions	41
Acknowledgment	43
References	43

<b>CHAPTER 3. SOME EFFICIENT BOUNDARY INTEGRAL STRATEGIES FOR WAVE PROBLEMS IN AN ELASTODYNAMIC HALFSPACE</b>	53
Abstract	53
Introduction	54
BIE Formulations	57
Truncation study for BIE Using the Stokes Solution	59
Lamb's Formulation Revisited	62
An Even More Efficient and Faster Strategy: the Library	63
Some Useful Approximations	65
Conclusions	67
Acknowledgment	68
References	69
<b>CHAPTER 4. PARALLEL IMPLEMENTATION OF A BOUNDARY ELEMENT ANALYSIS CODE FOR HALFSPACE ELASTODYNAMICS PROBLEMS</b>	80
Introduction	80
BIE Formulations	82
Serial Execution	84
Parallel Implementation	85
Conclusions	88
References	89
<b>CHAPTER 5. ELASTODYNAMIC SCATTERING FROM A SURFACE-BREAKING CRACK</b>	96
Introduction	96
Problem Description And the BIE Formulation	97
Discretization Considerations And Numerical Results	103
Partitioning Method and Library Idea	107
Discussion	109
References	110

<b>SUMMARY AND CONCLUSIONS</b>	123
<b>APPENDIX A. ELASTIC WAVE ANALYSIS SPHEROID (EWAS) LIBRARY USER'S MANUAL</b>	128
<b>APPENDIX B. COEFFICIENT MATRICES FOR COMPOSITE UNIT CELL</b>	145
<b>ACKNOWLEDGMENTS</b>	154
<b>VITA</b>	156

## **GENERAL INTRODUCTION**

### ***BIE/BEM***

The Boundary Integral Equation (BIE) formulation of boundary value problems (BVPs) in engineering, mathematics and applied science, and the Boundary Element Method (BEM) of solution of the integral equations has been an effective and popular approach for obtaining numerical data for real-world problems for more than thirty years. Mathematically, the boundary integral formulation can be traced back to the work of Green, Gauss, Fredholm and other classical mathematicians. It was Jaswon [1] and Symm [2] who first realized the new role that Green's boundary formula could play in the formulation and solution of practical problems in potential theory. Their work gave a new life to the study of integral equations and indicated the beginning of the so-called direct BIE method.

The work of Jaswon on potential theory was extended to elasticity theory in the 1960's by Rizzo [3]. In [3], the boundary integral equation for elasticity, known as the Somigliana's boundary formula [4], which is the vector counterpart of Green's formula, was solved using a similar collocation technique. This work and subsequent works on elasticity [5,6,7,8] started an era of applications of the BIE method in engineering fields and inspired a growing number of researchers to work in this area. In the late 1970's, the name BEM was given to this method in an attempt to make analogy with the Finite Element Method (FEM) (cf. several textbooks [9,10,11,12]). Since then, the method has experienced an increase in applicability, efficiency, and popularity. With the latest advances in computer technology, the BIEM/BEM has become a powerful numerical tool for analysis and design in almost every engineering

field. Detailed historical development and reviews of applications of the BIE/BEM can be found in the books and review articles [13,14,15].

### *Green's Functions*

Looking again at classical applied mathematics, the so called Green's function method [16,17] is among the oldest and most direct methods for solving BVPs governed by a linear elliptic partial differential equation. It is well known that an exact Green's function  $G^*$  exists and may be used, in principle, to construct the solution of a BVP governed by a linear elliptic partial differential equation for any reasonable domain. The only practical shortcoming with this simple and beautiful method is that it is not usually easy to find the Green's function explicitly for realistic geometries. Relatively few Green's functions exist, in explicit analytical form, and these are for fairly simple domains such as a halfspace, sphere, circular cylinder, etc. For more complex geometries or practical configurations, the Green's function is seldom available. Considerable effort has been expended, from time to time, to construct the Green's function in analytical, semianalytical or approximate forms, for certain specific problems; see for example Boley [18].

Now the main ingredient of BIEM/BEM is a Green's function, namely the simplest kind of Green's function, the so called freespace Green's function or fundamental solution to the governing partial differential equation. It is the use of this simplest Green's function which makes the most significant analytical step possible in the formulation of a BIE and in the derivation of integral representations for the desired fields in terms of boundary values. Since the two methods, BIEM/BEM and the Green's function method, are both methods for solving boundary value problems governed by a linear elliptic partial differential equation, and since

BIEM/BEM involves the freespace Green's function, there must exist a very close relationship between the two methods of solution. It is helpful to note in examining this relationship further, that every exact or region-dependent Green's function, which is usually so hard to construct, differs from the freespace one by a regular function  $w$ . Finding  $w$  is what is difficult for most domains. If this were not so difficult, there would be little need for numerical methods in general and the BIE/BEM in particular.

To continue the exploration of the mentioned relationship, some recent research on the BIEM/BEM and Green's functions [19,20,21] found that the exact Green's function and the unknown boundary variables on the boundary, in a given boundary value problem, satisfy the same BIE but with a different known vector. As a consequence, the representation integral for the BIE solution of the BVP may be written in a form which contains a precise expression for the exact Green's function. This observation provides a way to construct a numerical approximation to an exact Green's function (a discretized Green's function) for problems in which an analytical Green's function is not available. Indeed, it is apparent from Chapter 1 of this thesis that in using the BIE method to solve a given boundary value problem, one has in fact constructed the Green's function for the domain. A number of ingredients in the BEM may now be interpreted as numerical approximations to the exact Green's function. When using the BEM to obtain the discretized Green's function, there is no restriction on the configuration (2D or 3D), no restriction on boundary conditions, no restriction on the physical nature of the problem as long as it's a BVP governed by a linear elliptic partial differential equation. All of the BVPs considered in this thesis are in this category.

It is shown in Chapter 1 that for a BVP for a domain bounded by a single surface, the inverse of the coefficient matrix ( $A^{-1}$ ) is closely related to the discretized Green's function for the BVP. The construction of this inverse is the key and most computationally-intensive ingredient in the usual BEM solution of a BVP. The BEM solution requires a mesh, a comprehensive computer code and all of the expertise to make the meshes and use the code in order to get reliable solutions. The computer solution process itself involves mainly matrix multiplications based on well established formulas for numerical quadrature.

Therefore, why not consider forming and storing at least  $A^{-1}$ , for common and/or important boundary shapes and/or boundary conditions? This could be done by computer-modeling experts. In effect, why not create a '*library*' of numerical approximations to exact Green's functions to be available for repeated use? Modern technology for storage of massive amounts of data, on CDs or on central storage, accessible via networks, would suggest that at least some heavy computing could be 'done in advance', the results of which could be made available to non expert users. Such users, interested mainly in the data for particular physical problems, could get such data, via 'point and click' operations, in negligible time - the expert modeling, i.e., creating the Green's function library, having been done in advance by others.

Details about the relation between  $A^{-1}$  and the discretized Green's function, for BVPs with single surface boundary and strategies for using the discretized Green's function to obtain the solution to the BVP are addressed in Chapter 1. For problems which involve two separate surfaces as the boundary, a sub-matrix of the coefficient matrix can be interpreted as the main ingredient of the region dependent Green's function. The process of using this region dependent Green's function is closely related to the partitioning method [20]. Thus for

problems with two surfaces as the boundary, such as halfspace problems, the library idea is closely related to the partitioning of the system matrix. In Chapter 3, the library idea for halfspace problems using freespace fundamental solution amounts to: giving an accurate discretization of the halfspace free surface, obtaining the coefficient sub-matrix for the truncated halfspace surface model, and then storing its inverse (in fact the LU decomposition of that coefficient sub-matrix) for repeated use.

### *Applications*

In this thesis, two classes of problems are considered as applications of the BEM and the discretized Green's function library. One is the application of the BEM to the analysis of 2D micromechanical behavior of fiber-reinforced composites. With the rapid development of advanced composite materials and the wide application of such materials in engineering, it is desirable to model problems involving these materials by computer and to use powerful numerical methods like the Finite Element Method (FEM) and the BEM for analysis. To exploit the role of BEM and Green's functions for computer modeling of advanced materials properties and behavior, a BEM model is developed to analyze 2D micromechanical behavior of fiber-reinforced composites based on models for both perfectly-bonded and imperfectly-bonded materials in a unit cell. The idea of a library of Green's functions and the entries for the library for fiber-reinforced composites are discussed.

The other class of problems considered here is the halfspace problem. The BEM is well known for its well-suitedness for exterior problems. With the (radiation) conditions on the surface at infinity incorporated analytically, only finite surface(s) need to be discretized when the only other surface(s) in the problem are finite in extent.

When BIE/BEMs are used for halfspace problems, such as occur frequently in elastodynamics, fullspace (Stokes) fundamental solution and halfspace (Lamb) fundamental solution can be used to formulate the BIE. When the fullspace fundamental solution is used, a truncated discretized model of the halfspace surface is required. Alternatively, if the halfspace fundamental solution, which models the entire halfspace surface analytically is used, no truncation issues arise. Nevertheless, both Stokes and Lamb approaches have advantages and disadvantages.

The purposes of the application of the BEM to this class of problems are first to present systematic strategies, based on the BEM for halfspace elastodynamics problems, wherein the best features of the fullspace Stokes solution and halfspace Lamb's solution are exploited, and then to present library strategies for this class of problem which represent the typical two-surface problem.

Radiation from a void inside the halfspace and the scattering from a halfspace surface-breaking crack are considered in this thesis. Although they all belong to the halfspace-problem category, the necessity to use hypersingular integral equations for the crack problem brings in more complexity both theoretically and numerically. Nevertheless the conclusions about effective strategies for both problems are quite consistent. Specifically, when the fullspace fundamental solution is used in the BIE formulation, the truncation on the halfspace surface has a small effect on the boundary solution and quite a big effect on the solution at field points. So in order to get a reliable solution at field points, the halfspace Green's function rather than the fullspace one is advised to be used in the representation integral.

## *Dissertation Organization*

The body of this dissertation consists of five main chapters, a general introduction, a summary and general conclusions, as well as two appendices. The five chapters consist of one chapter which is a blend of two papers presented in technical conferences, three chapters which are accepted or submitted or prepared for journal paper manuscripts, and a fifth chapter which contains some relevant important research information. Because of the inclusion of manuscripts, all the labels for the equations, figures, tables and references are numbered independently. All the references for each main chapter are at the end of each chapter and each follows the required format for the particular journal. A general reference which contains the citation in the general introduction is at the end of the general introduction. All the figures are at the end of the manuscripts, just as they are in the manuscript sent to the journal. This structure follows the format requirement for a thesis including journal manuscripts.

Chapter 1 is a blend of two papers which appear in the proceedings of the BEM IVII Conference and 24th Midwest Mechanics Conference. It is entitled “Exact Green's functions and the boundary element method” in which the precise equivalence between an exact Green’s function and the solution of the boundary integral equation is illustrated and made explicit. Some strategies about how to use the discretized Green’s function to obtain the solution of the problem are suggested. Numerical examples using these strategies are also presented.

Chapter 2 is a paper accepted and to appear in the journal *Computers & Structures*. It is entitled “BEM analysis for composite materials and a library of Green's functions”. In this paper a BEM model is developed to analyze 2D micromechanical behavior of fiber-reinforced

composites based on models for both perfectly-bonded and imperfectly-bonded materials in a unit cell. Also some suggestions for a Green's function library, for this class of problems, are given.

Chapter 3 is a paper submitted to *Computer Methods in Applied Mechanics and Engineering*. It is entitled "Some efficient boundary integral strategies for wave problems in an elastodynamic halfspace". Here, both fullspace (Stokes) fundamental solution and halfspace (Lamb) fundamental solution are used to formulate the BIE to attack the halfspace problem. Some new insight into this class of problems was gained during the research. Strategies are suggested to exploit the best features of the fullspace Stokes and halfspace Lamb solutions. The partitioning method is also implemented and the efficiency of the library is demonstrated.

Chapter 4 is a continuation of the work done in Chapter 3. A 'coarse-grained' parallel-computing scheme is designed and implemented to cope with the intensive computational work when the halfspace Green's function is used in the BIE formulation. A 'nearly perfect' speedup is obtained and this indicates that BIE/BEM is very well suited for parallel computing.

Chapter 5 is about a slightly different halfspace-scattering problem. It involves elastodynamic scattering from a surface-breaking crack. A hypersingular boundary integral equation (HBIE) is introduced and used because of the presence of the crack. A consistent conclusion with that in Chapter 3 is obtained, i.e., truncation on the halfspace surface, as needed for the use of the fullspace fundamental solution, has little effect on the boundary

solution, while it has a big effect on the solution at field points. Results are presented in the form of crack-opening displacement (COD), and farfield scattering amplitudes.

Additionally, there is an Appendix A which is a user's manual entitled 'Elastic wave analysis spheroid (EWAS) library user's manual'. This material is included to illustrate the library idea of discretized Green's functions, for single-surface problems. This scattering library has been constructed for elastodynamic scattering from families of oblate-spheroidal voids, of various eccentricities, for waves of different frequencies. With this library, the elastodynamic scattered field at arbitrary points, from shapes and frequencies in the library, due to arbitrary incident waves, is just a matter of matrix multiplication. This finds use by physicists engaged in nondestructive evaluation at Iowa State University.

Finally, Appendix B contains all of the detailed information about the coefficient matrices for composite analysis, using either an entire-cell model or a one-quadrant model, which is not presented in Chapter 3.

### *References*

1. M.A. Jaswon, Integral equation methods in potential theory, I, Proc. Royal Soc., A, 275 (1963) 23-32.
2. G.T. Symm, Integral equation methods in potential theory, II, Proc. Royal Soc., A, 275 (1963) 33-46.
3. F.J. Rizzo, An integral equation approach to boundary value problems of classical elastostatics, Quart. Appl. Math., 25 (1967) 83-95.
4. A.E.H. Love, A Treatise on the Mathematical Theory of Elasticity (Dover, New York, 1944).

5. T.A. Cruse, F.J. Rizzo, A direct formulation and numerical solution of the general transient elastodynamic problem I, *Journal of Math. Analysis and Applications*, 22 (1968) 244-259.
6. T.A. Cruse, A direct formulation and numerical solution of the general transient elastodynamic problem II, *Journal of Math. Analysis and Applications*, 22 (1968) 341-355.
7. T.A. Cruse, Numerical solutions in three dimensional elastostatics, *Int. J. Sol. Structs.*, 5 (1969) 1259-1274.
8. T.A. Cruse, An improved boundary-integral equation method for three-dimensional elastic stress analysis, *Computes. and Structs.*, 4 (1974) 741-754.
9. C.A. Brebbia, *The Boundary Element Method for Engineers* (Pentech Press, London, 1978).
10. P.K. Banerjee, R. Butterfield, *Boundary Element Method in Engineering Science* (McGraw-Hill, New York, 1981).
11. P.K. Banerjee, et al. (eds.), *Developments in Boundary Element Methods, Vols. I to VII* (Elsevier Applied Science Publishers, London, 1979-1991).
12. C.A. Brabbia, J.C.F. Telles, L.C. Wrobel, *Boundary Element Techniques* ( Computational Mechanics Publications, Southampton, UK, 1984).
13. F.J. Rizzo, The boundary element method, some early history--A personal view, In D.E. Beskos, eds., *Boundary Element Methods in Structural Analysis*, (ASCE, 1989).
14. J. Trevelyan, *Boundary Elements for Engineers, Theory and Applications* (Computational Mechanics Publications, Southampton, UK, 1994).

15. M. Tanaka, Some recent advances in boundary element methods, *Appl. Mech. Revs.*, 36 (5) (1983), 627-634.
16. O.D. Kellogg, *Foundations of Potential Theory* (Springer, Berlin, 1929).
17. M.D. Greenberg, *Application of Green's Functions in Science and Engineering* (Prentice-Hall, New Jersey, 1971).
18. B.A. Boley, A method for the construction of Green's functions, *Q. Appl. Math.*, 14 (1956), 249-257.
19. D.E. Budreck, A discretized Green's function for an elastodynamic crack, preprint, 1994.
20. P.A. Martin, & F.J Rizzo, Partitioning, boundary integral equations, and exact Green's functions, *Int. J. for Num. Meth. in Engrg*, 38 (1995) 3483-3495.
21. F.J. Rizzo, P.A. Martin & R.A. Roberts, Boundary elements and a Green's function library, *Proceedings of NIST Workshop on Green's Functions and Boundary Element Analysis for Modeling of Mechanical Behavior of Advanced Materials*, Boulder, Colorado, 1994.
22. D.E. Budreck and J.D. Achenbach, Scattering from three-dimensional planar cracks by the boundary integral equation method, *J. Appl. Mech., Trans. ASME* 55(2) (1988), 405-412.

GENERAL INTRODUCTION.....	1
BIE/BEM .....	1
Green's Functions.....	2
Applications.....	5
Dissertation Organization.....	7
References .....	9

**CHAPTER 1**

**EXACT GREEN'S FUNCTIONS AND THE BOUNDARY**

**ELEMENT METHOD**

A paper presented at 24th Midwest Mechanics Conference

Lingyun Pan and Frank J. Rizzo

Department of Aerospace Engineering and Engineering Mechanics

Iowa State University, Ames, IA 50011

***Introduction***

It is well known, e.g. Kellogg [1], Webster [2], that an exact Green's function  $G^*$  exists and may be used, in principle, to construct the solution of a boundary value problem governed by a linear elliptic partial differential equation. Alternatively, the solution of the problem may be obtained via the boundary integral equation (BIE) formalism, where the BIE employs only the free-space Green's function  $G$  or fundamental solution of the differential equation. Since it is evident that both approaches to the solution must be equivalent [3], one may conjecture that, using the BIE one must have done the equivalent of constructing the exact Green's function  $G^*$ .

Indeed, here (see also [4],[5],[6]) it is explicitly shown that  $G^*$  and the unknown boundary variable in the BIE method satisfy the same BIE, but with different right-hand sides.

As a consequence, the representation integral for the BIE solution of the boundary value problem may be written in a form which contains a precise expression for  $G^*$ . The equivalence between the BIE process and constructing  $G^*$  is thus made explicit.

A number of ingredients in the boundary element method (BEM) may now be interpreted as numerical approximations to exact Green's functions. Some strategies for creating a library of such functions for repeated use are suggested.

### ***Exact Green's Functions and the BIE Process***

The essential aspects of the following arguments hold for linear elliptic boundary value problems (BVP's); however, to fix ideas, consider finding a time-harmonic acoustic field  $u$  which exists in the region  $D$  exterior to a single finite volume  $V$  with closed surface  $S$  as in Figure 1.

The field  $u$  satisfies the scalar wave (Helmholtz) equation in  $D$  and satisfies a radiation condition for indefinitely large distance  $R$  from  $V$ . On  $S$  we assume  $\nabla u / \nabla n = f$  where  $f$  is a prescribed function. A representation integral for  $u$  may be written

$$2u(P) = \int_S [f(q)G(q, P) - u(q) \frac{\nabla G(q, P)}{\nabla n_q}] dS_q \quad (1)$$

wherein

$$G(P, Q) = G(Q, P) = \frac{-e^{ikR}}{2pR} + w(P, Q) \quad (2)$$

is a Green's function with  $R = |Q - P|$ , where  $P, Q$  are arbitrary points in  $D$  and  $p, q$  are arbitrary points on  $S$ ;  $k$  is the acoustic wavenumber,  $w$  is an arbitrary regular solution to the

wave equation, and the normal  $n$  points into  $D$  at  $q$ . Equation (1) is readily obtained by inserting  $u$  and  $G$  into Green's reciprocal identity.

Now suppose that  $G$  in eqn (1) is an exact Green's function  $G^*$  defined such that

$$\frac{\mathcal{I}G^*(q, P)}{\mathcal{I}n_q} = 0 \quad \text{or} \quad \frac{\mathcal{I}}{\mathcal{I}n_q} \left( \frac{-e^{ikR}}{2pR} \right) + \frac{\mathcal{I}w(P, q)}{\mathcal{I}n_q} = 0 \quad (3)$$

whenever  $q \in S$ . Using  $G^*$  instead of  $G$ , representation (1) simplifies considerably to

$$2u(P) = \int_S f(q)G^*(q, P)dS_q \quad (4)$$

which is now the explicit solution to the posed BVP rather than a mere representation, if  $G^*$  is assumed known, since unprescribed  $u(q)$  does not appear in (4).

Note that finding  $G^*$  is tantamount to finding  $w$  which satisfies the wave equation subject to the boundary condition (3). This task is comparable in difficulty to finding  $u$  itself subject to  $\mathcal{I}u/\mathcal{I}n = f$ . This is why, no doubt, the idea of an exact Green's function has not received more attention for practical problems.

Instead, the BIE/BEM has been the method of choice for many problems of the present type, and the method, in essence, proceeds as follows. Choose the simplest  $w$  in (2), namely  $w = 0$ , and take the limit in representation (1) as  $P \rightarrow p$ . The familiar result is the BIE

$$u(p) + \int_S u(q) \frac{\mathcal{I}G(q, p)}{\mathcal{I}n_q} dS_q = \int_S f(q)G(q, p)dS_q. \quad (5)$$

Symbolically, eqn (5) may be written

$$Au = Bf \quad (6)$$

where  $A$  and  $B$  are the indicated integral operators. The unknown function  $u$  on  $S$  may be obtained formally as the solution of the BIE, namely

$$u = A^{-1}Bf. \quad (7)$$

Thus, using (7) we may write the solution for  $u(P)$  as

$$2u(P) = \int_S f(q)G(q,P)dS_q - \int_S \underbrace{A^{-1}Bf(q)}_u \frac{\mathcal{I}G(q,P)}{\mathcal{I}n_q} dS_q. \quad (8)$$

Comparing (8) with (4), we find two representations for the solution to our boundary value problem; (8) explicitly involves the inverse operator  $A^{-1}$  acting upon the function  $Bf$ , whereas, (4) explicitly involves the exact Green's function  $G^*$ .

To more closely see the equivalence between (8) and (4), it is instructive to reintroduce the integral form of the operator  $Bf$  into (8), and in the process interchange the order of the inner integration with the operation  $A^{-1}$ . The result is

$$2u(P) = \int_S f(q)G(q,P)dS_q - \int_S f(q) \left\{ \int_S A^{-1}G(q,l) \frac{\mathcal{I}G(l,P)}{\mathcal{I}n_l} dS_l \right\} dS_q \quad (9)$$

where  $l \in S$ . Next, factoring out a common  $f(q)$  we have

$$2u(P) = \int_S f(q) \left[ G(q,P) - \int_S A^{-1}G(q,l) \frac{\mathcal{I}G(l,P)}{\mathcal{I}n_l} dS_l \right] dS_q. \quad (10)$$

Now if (10) and (4) are both correct, the term in brackets in (10) must be  $G^*$

To see that the term in brackets is, in fact,  $G^*$ , apply Green's reciprocal theorem to  $G$  and  $G^*$ , to get

$$2G^*(P,Q) = 2G(P,Q) - \int_S G^*(l,P) \frac{\mathcal{I}G(l,Q)}{\mathcal{I}n_l} dS_l \quad (11)$$

where we recall that  $\mathcal{I}G^*(l,P)/\mathcal{I}n = 0$ . Next take the limit in (11) as  $Q \rightarrow s \in S$  to get (cf. Boley [5])

$$G^*(P, s) + \int_S G^*(l, P) \frac{\mathcal{I}G(l, s)}{\mathcal{I}n_l} dS_l = 2G(P, s) \quad (12)$$

or symbolically

$$AG^* = 2G. \quad (13)$$

From (12) (and (13)) and (6) (and (7)) we see that both  $u$  and  $G^*$  satisfy the same BIE with different right hand sides. Solving (13) for  $G^*$  as (cf. Tewary [6])

$$G^* = 2A^{-1}G \quad (14)$$

and substituting under the integral sign in (11), we obtain, after interchanging  $P$  with  $Q$  (or  $q$ )

$$G^*(P, q) = G(P, q) - \int_S A^{-1}G(l, q) \frac{\mathcal{I}G(l, P)}{\mathcal{I}n_l} dS_l. \quad (15)$$

Expression (15) for  $G^*$  is precisely that in brackets in equation (10) such that (10) and (4) are identical.

*It is explicit, therefore, that in using the BIE method to solve a given boundary value problem for the scalar wave equation, one has in fact constructed the Green's function for the domain. The key ingredient in both methods is the solution to essentially the same BIE, which is expressible as  $A^{-1}$ .*

### ***Some Approximate Forms and Solution Strategies***

From the observations above, the boundary element method may be thought of as a systematic way of approximating the BIE (6) by systems of algebraic equations. In so doing,  $A$  and  $B$  may be interpreted as (square) matrix approximations to the integral operators based on a discretization of the domain surface  $S$ , with  $u$  and  $f$  familiar (column matrix) numerical approximations to the continuous boundary variables.

Therefore, it is clear that for a given discretization, we may form and invert a matrix  $A$ , and via (14), we would have an approximate representation for  $G^*(q_N, P)$  for a given choice of surface nodes  $q_N$ . To use this  $G^*(q_N, P)$  to get the solution  $u(P)$  based on (4), it would be necessary to get representations for  $G^*(q_G, P)$  at Gaussian quadrature points  $q_G$ , in order to do the quadrature indicated in (4) numerically. That quadrature is expressible in the form

$$2u(P) = G^*(P, q_G)f(q_G). \quad (16)$$

In (16),  $f(q_G)$  is a column of discrete values of  $f$  at the Gauss points  $q_G$  on  $S$  and  $G^*(P, q_G)$  is a row matrix of values of Gauss-weighted  $G^*$  evaluated at the same  $q_G$  for chosen  $P$ . To get the values of  $G^*$  at the Gauss points from values at nodal points, interpolation using shape functions were employed. There are two strategies for doing the interpolation.

One is to interpolate the product of  $f$  and  $G^*$  as:

$$f(q_G)G^*(q_G, P) = \sum_{i=1}^8 N_i f(q_{Ni})G^*(q_{Ni}, P). \quad (17)$$

The other is to interpolate  $f$  and  $G^*$  separately as

$$f(q_G) = \sum_{i=1}^8 N_i f(q_{Ni}), \quad (18)$$

$$G^*(q_G, P) = \sum_{i=1}^8 N_i G^*(q_{Ni}, P). \quad (19)$$

It seems that the second strategy might give better results than the first strategy. This matter is addressed further in the numerical examples to follow.

### *Numerical Examples*

In order to illustrate the idea of a discretized Green's function and the strategies for using a discretized Green's function, several numerical examples are discussed . The first one is the problem of sound radiation from a pulsating sphere (See Figure 2).

The exact analytical solution for the acoustic pressure at a distance  $r$  from the center of the sphere of radius  $a$  pulsating with a uniform radial velocity  $U_a$  is:

$$p(r) = \frac{a}{r} U_a \frac{iZ_0ka}{1+ika} e^{-ik(r-a)} . \quad (20)$$

where  $Z_0$  is the characteristic impedance of the medium.

The pressure at two interior points at different radial locations ( $r=5a$ ,  $r=10a$ ) are calculated. Table 1 shows the results from conventional BIE (see eqn (8)), from strategy 1(see eqn (17)) and strategy 2(see eqn (18)) by using the discretized Green's function.

The same accuracy is obtained by strategy 1 and 2 because this problem has a spherical symmetry which makes the field uniform over all elements. The interpolation in both strategies 1 and 2 do not introduce any approximation error.

In another example, a uniform flow over a sphere is considered (See Figure 3). The velocity potential  $\Phi$  satisfies Laplace's equation. To satisfy the condition at infinity, the potential  $\Phi$  is divided into two parts,  $\Phi_1$ ,  $\Phi_2$

$$\Phi = Ur_0 \cos \mathbf{q} \left[ \frac{r}{r_0} + \frac{1}{2} \left( \frac{r}{r_0} \right)^{-2} \right] = \Phi_1 + \Phi_2 \quad (21)$$

$$\Phi_1 = Ur \cos \mathbf{q} \quad (22)$$

Table 1 Magnitude of the pressure in the field

Location	From CBIE	From $G^*$	
		Strategy 1 (eqn 17)	Strategy 2 (eqn 18)
$r = 5 a$	0.141	0.141	0.141
$r = 10 a$	0.0705	0.0707	0.0707

$$\Phi_2 = \frac{1}{2} U r_0 \cos \theta \left( \frac{r}{r_0} \right)^{-2} \quad (23)$$

where  $\Phi_1$  is the velocity potential associated with the uniform stream, while  $\Phi_2$  the velocity potential associated with the doublet,  $U$  is the velocity of the flow. So in the BEM calculation, only the doublet  $\Phi_2$  which is zero at infinity is calculated as the solution to the BVP when  $\frac{\partial \Phi_2}{\partial n}$  is specified over the entire boundary (on the surface of the sphere). The results in Table 2 confirmed that strategy 2 is better than strategy 1, but when a finer mesh is used, they all converge to the results from the CBIE.

### ***An Alternative for Getting the Discretized Green's Function from the CBIE***

As a more familiar alternative to (16), we have the approximate form of (1) that comes directly from the BEM as usually coded, i.e.,

Table 2 Comparison between CBIE, strategy 1 and 2 for fluid flow problem

Point	Coordinates		Analytical solution for $\Phi_2$	12 elements mesh results			80 element mesh results		
	$r$	$q$ (degrees)		CBIE	Strategy 1	Strategy 2	CBIE	Strategy 1	Strategy 2
A	1.5	150	-0.19259	-0.15797	-0.15926	-0.16544	-0.18603	-0.18639	-0.18630
B	1.5	120	-0.11111	-0.09182	-0.06612	-0.08175	-0.10906	-0.10858	-0.10859
C	2	150	-0.10813	-0.08921	-0.09000	-0.09093	-0.10497	-0.10506	-0.10504
D	2	120	-0.06250	-0.05162	-0.04501	-0.04860	-0.06131	-0.06104	-0.06106

$$2u(P) = G(P, q_G)f(q_G) - G^n(P, q_G)u(q_G) \quad (24)$$

where the superscript  $n$  indicates the normal derivative of  $G$  and, wherein,

$$u(q_N) = A^{-1}Bf(q_N). \quad (25)$$

In (25), function values at  $q_G$  are given in terms of values at  $q_N$  via the shape functions.

Thus, it is possible to factor out  $f$  in (25), to write

$$2u(P) = \{G(P, q_G) - G^n(P, q_G)CA^{-1}BC^T\}f(q_G) \quad (26)$$

where  $C$  and  $C^T$  are rectangular matrices dependent upon the shape functions and coordinates  $q_G$ . In (26) we can identify an approximate form of  $G^*$  as the term in brackets, just as we did with the comparable analytical expressions. The bracket-term in (26) is equivalent in character to  $G^*$  in (16), but there is an important strategic difference: to get  $G^*$  values at  $q_G$  (for chosen  $P$ ), in (16) requires some kind of approximate representation of  $G^*$  over  $S$ , as mentioned above; whereas comparable  $G^*$  values via (26) or (24) require no such representation. Indeed, since both  $G$  and  $G^n$  in (26) and (24) have analytical form, each may readily be evaluated anywhere. Specifically, since with the conventional BEM,  $u(q_N)$  is obtained via (25), only  $u(q_G)$  need be expressed as usual, with standard shape functions, in terms of nodal values. Thus (24) rather than (26) is usually used by the BEM community to get  $u(P)$ . To exploit the apparent simplicity of (16), with its need for perhaps special representations of  $G^*$ , versus the more complicated (24) or (26), emanating from the standard BIE with no such need, deserves more study. Either way, it is possible, with today's technology, to take the following somewhat radical point of view.

### *The Library Idea*

The key and most computationally-intensive ingredient in the usual BEM solution of a BVP of the present type is the construction of  $A^{-1}$ . This requires a mesh, a code to form  $A$  and  $B$ , and then the effort to find  $A^{-1}$  (or, equivalently, the LU decomposition of  $A$ ). The rest of the solution process involves mainly matrix multiplication based on formulas for numerical quadrature. Therefore, why not consider forming and storing at least  $A^{-1}$ , and possibly  $B$  (depending on the tradeoff on using (16) versus (24) or (26)), for common and/or important shapes  $S$ ? In effect, why not create a library of numerical approximations to exact Green's functions for repeated use?

Modern technology for storage of massive amounts of data, on CDs or on central storage, accessible via networks, would suggest that such a library is now possible. At least some heavy computing could be 'done in advance', the results of which could be made available to non expert users via the library.

Some details for the formation of a Green's function library may be found in [4] and [7]. Also, a library of  $A^{-1}$  matrices has been constructed for elastodynamic scattering [8] from families of oblate-spheroidal voids, of various eccentricities, for waves of different frequencies. With this library, the elastodynamic scattered field at arbitrary points, from shapes and frequencies in the library, due to arbitrary incident waves, is just a matter of matrix multiplications. Library entries for other scatters, e.g., cracks, inclusions, are already in existence or are being formed - all of which find use by physicists engaged in nondestructive evaluation at Iowa State University. Partially-exact Green's functions, which model only (a common or especially complicated) part of a surface are also being

formed, for repeated use, for fiber reinforced composites, acoustic and electromagnetic field problems. Much unnecessary duplication in computing can be avoided in this way.

Additional reference and information about the library idea for specific applications may be found in subsequent chapters of this thesis.

### *References*

1. Kellogg, O.D. *Foundations of Potential Theory*, Springer, Berlin, 1929.
2. Webster, A.G. *Partial Differential Equations of Mathematical Physics*, Dover, New York, 1964.
3. Budreck, D.E. A Discretized Green's Function for an Elastodynamic Crack, *preprint*, 1994.
4. Martin, P.A. & Rizzo, F.J. Partitioning, Boundary Integral Equations, and Exact Green's Functions, *International Journal for Numerical Methods in Engineering* (to appear).
5. Boley, B.A. A Method for the Construction of Green's Functions, *Q. Appl. Math.*, 1956, **14**, 249-257.
6. Tewary, V.K. Green's Function Method for Lattice Statics, *Advances in Physics*, 1973, **22**, 757.
7. Rizzo, F.J., Martin, P.A. & Roberts, R.A. Boundary Elements and a Green's Function Library, *Proceedings of NIST Workshop on Green's Functions and Boundary Element Analysis for Modeling of Mechanical Behavior of Advanced Materials*, Boulder, Colorado, 1994.

8. Pan, L. EWAS Scattering Library User's Manual, AEEM Dept. Report, Iowa State University, 1994.
9. Zhang, D. Sensitivity BIE with Applications to Fracture Mechanics, Shape Optimization, and Flaw Detecting, *PhD Thesis*, Department of AEEM, Iowa State University, 1997.

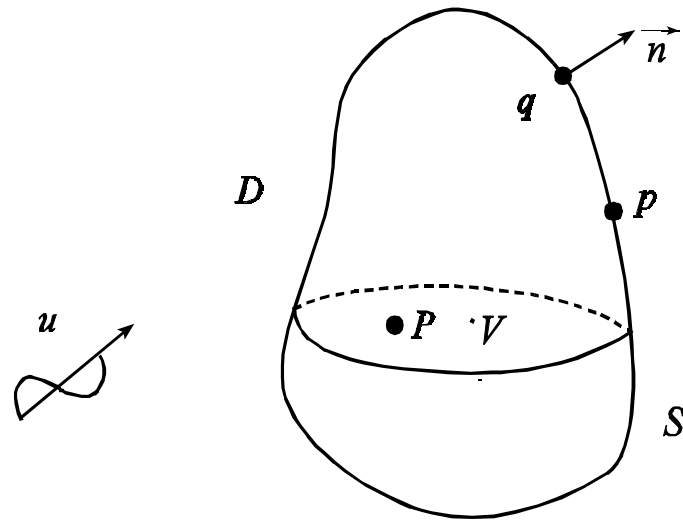


Figure 1 An acoustics example

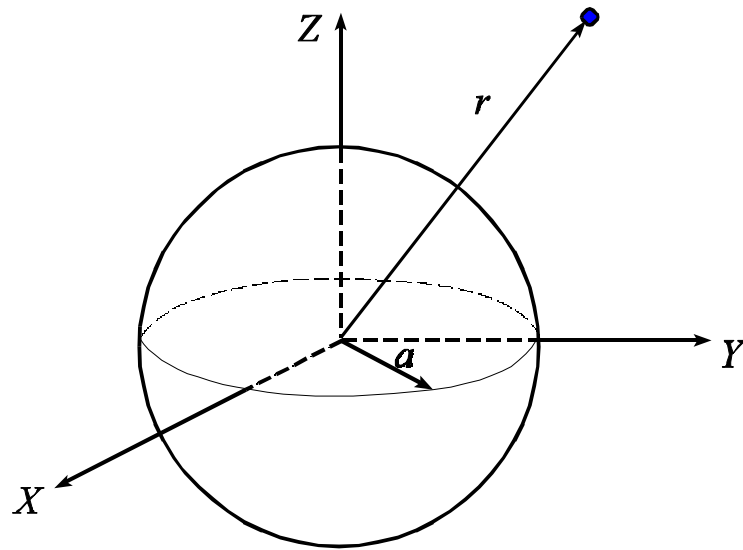


Figure 2 Sound radiation from a pulsating sphere

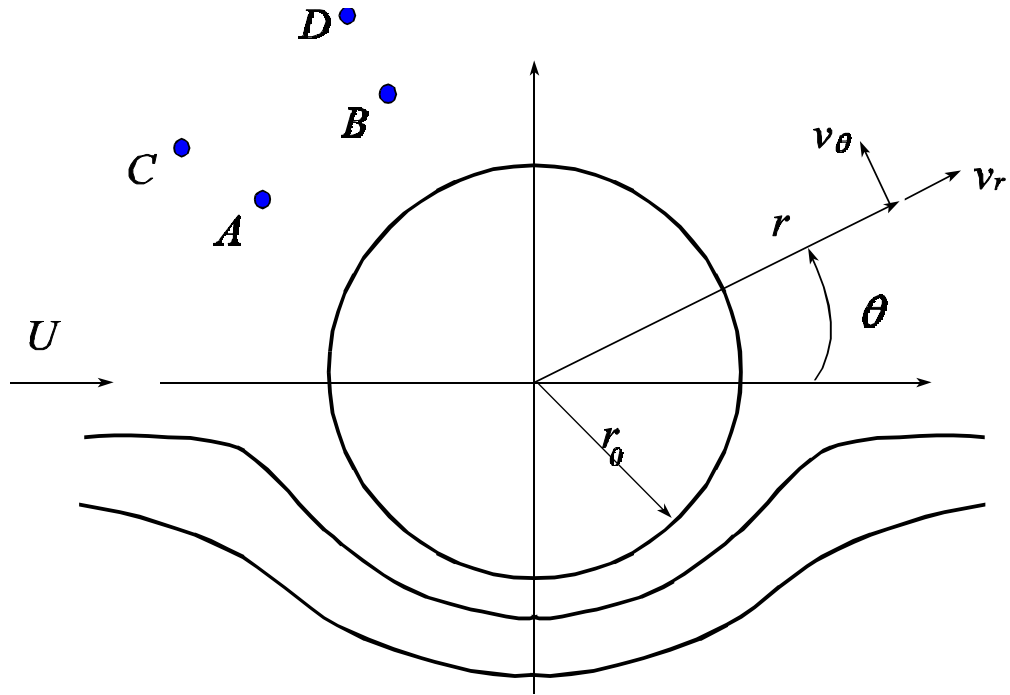


Figure 3 Uniform flow over a sphere

CHAPTER 1 EXACT GREEN'S FUNCTIONS AND THE BOUNDARY ELEMENT METHOD .....	12
Introduction.....	12
Exact Green's Functions and the BIE Process.....	13
Some Approximate Forms and Solution	
Strategies.....	16
Numerical Examples .....	18
An Alternative for Getting the Discretized	
Green's Function from the CBIE .....	19
The Library Idea .....	22
References .....	23
 Figure 1 An acoustics example.....	 25
Figure 2 Sound radiation from a pulsating sphere .....	26
Figure 3 Uniform flow over a sphere.....	27

**CHAPTER 2**

**BEM ANALYSIS FOR COMPOSITE MATERIALS AND A  
LIBRARY OF GREEN'S FUNCTIONS**

A paper to appear in the journal Computers and Structures

Lingyun Pan, Daniel O. Adams, Frank J. Rizzo

Department of Aerospace Engineering and Engineering Mechanics

Iowa State University, Ames, IA 50011

***Abstract***

With the rapid development of advanced composite materials and the wide application of such materials in engineering, it is desirable to model problems involving these materials by computer and to use powerful numerical methods like the Finite Element Method (FEM) and the Boundary Element Method ( BEM ) for analysis. In this paper, a BEM is developed to analyze 2D micromechanical behavior of fiber-reinforced composites based on models for both perfectly-bonded and imperfectly-bonded materials in a unit cell. For composites with perfect bond between matrix and fibers, it is shown that our predictions coincide well with comparable quantities obtained in physical experiments and by FEM analysis. For imperfectly-bonded composites, it is found that variation of the interphase parameters (thickness, stiffness) causes pronounced changes in the overall effective moduli and also in the state of stress in the

composites. Also in this paper, the idea of a library of Green's Functions for fiber-reinforced composites is discussed. With such a library, users could quickly generate data useful in design with very little knowledge of methods for computational modeling in general or of the BEM in particular.

## ***1. Introduction***

Considerable research has been done on the analysis of the micromechanical properties of fiber reinforced composites since the development of advanced composite materials. Perhaps the most widely used analytical approach for estimating the properties of composite materials is the rule of mixtures, which can reasonably predict Young's and shear moduli of the composite material when the composite has a strong bond between fiber and matrix. However the perfect bonding assumption is not suitable in the presence of an interphase, which may have developed during the manufacturing process due to chemical reactions between the contacting fiber and matrix material. Also, surface treatments are typically applied to the fibers to improve interface sensitivity composite material properties, but an analytical estimation of the influence of surface treating has not been available to people involved in surface studies.

Several finite element models have been developed for the purpose of considering the presence of an interphase [1, 2]. Among these is the finite element model developed by Adams at the University of Wyoming [1], in which an additional layer of very fine finite elements was used at the fiber-matrix interface to model the interphase zone. Thus, the unit cell of the composite basically consists of three different materials (fiber, matrix and interphase zone).

There also has been some research done on the analysis of the micromechanical properties of fiber reinforced composites using the Boundary Element Method [3,4] with the usual well-known advantages of reduction of dimension by one. That is, with the BEM, only the boundary needs to be discretized. Further, for the purpose of determining overall effective moduli, the information in the domain generated by FEM is not really required. Thus, the same level of accuracy for the desired information can be achieved by BEM vs. FEM with less computational effort. In both Refs. [3] and [4] constant boundary elements were used and good agreement with analytical solutions were found. Furthermore it was shown that the BEM is very effective when an imperfect interface condition is considered [4]. However, as there seems to be no user-friendly BEM software in wide use by the composite community, the power of this numerical method has been restricted.

One purpose of our research is to develop a BEM to analyze two-dimensional micromechanical behavior of fiber-reinforced composites based on models for both perfectly-bonded and imperfectly-bonded materials in a unit cell. Another purpose is to eventually form a library of Green's Functions for the most-needed and most-often-used fiber volume fractions, fiber/matrix combinations and interphase conditions as (possibly) identified by the composite-materials community. With this Green's function library, users in the community could determine the effects of design parameters (e.g. to establish effective coating-thicknesses for fibers) and the effects of damage and different manufacturing processes on the overall mechanical properties of fiber-reinforced composites. With the library, all of this could be done with very little knowledge of methods for computational modeling in general, or of the BEM in particular. Most significant, perhaps, is that with all of the heavy computing and

the expertise needed for that computing exercised in advance, and results put in storage for repeated use, the mentioned analysis could be performed with negligible user effort in negligible time.

Specifically in this paper, a BEM is developed to analyze two-dimensional micromechanical behavior of fiber-reinforced composites based on models for both perfectly-bonded and imperfectly-bonded materials in a unit cell. For composites with perfect bond between matrix and fibers, it is shown that such quantities as the overall effective moduli, displacement field, and state of stress, as computed with the BEM, coincide well with comparable quantities obtained in physical experiments and by FEM analysis. For imperfectly-bonded composites, a model is used with continuous tractions across the interface and a linear relation between displacement differences and the conjugate tractions across the interface. It is found that variation of the interphase parameters (thickness, stiffness) causes pronounced changes in the overall effective moduli and also in the state of stress in the composites.

## ***2. Method of Analysis***

The composite material is assumed to consist of a square array of unidirectionally oriented fibers in an infinite elastic matrix as shown in Fig. 1. Assuming a square fiber packing array, the composite material could be represented by a unit volume cell as indicated by the dashed lines in Fig. 1 and 2(a), or even by only one quadrant of the unit cell, if the loading condition is also symmetric as shown in Fig. 2(b). For consistency and conciseness, the entire unit cell model will be used in this paper, while the method of analysis also applies to the one-quadrant model in the calculation of effective tension modulus. In the one-quadrant model, symmetries could be utilized to set the boundary conditions.

The composite body is assumed to be loaded at infinity. For example, to determine the effective transverse tension modulus, the body is assumed to be loaded at infinity by uniform normal stress  $\mathbf{S}_0$  in the  $x$  coordinate direction, as shown in Fig. 1. When the composite is subjected to transverse normal load applied at a distance from the element being analyzed, a complex state of stress is induced in the composite. This is the result of the dissimilar material properties for the fiber and the matrix and also because of interactions between the fiber being analyzed and adjacent fibers. Thus, the stress distribution along the boundary of the unit cell will not be uniform, although the average normal stress must equal the corresponding average applied stress from equilibrium considerations. However, because of symmetry, the original square unit cell remains rectangular when only transverse normal load is applied. Thus the normal displacement of each point on a given boundary of the unit cell is identical. Because of the assumed symmetry about both coordinate axes, no shear stress exist along the boundaries of the unit cell, thus the boundary conditions are specified as

$$\begin{aligned}
 u_x = 1 \quad t_y = 0 & \quad \text{on } AB \\
 t_x = 0 \quad u_y = -C/2 & \quad \text{on } BC \\
 u_x = 0 \quad t_y = 0 & \quad \text{on } CD \\
 t_x = 0 \quad u_y = C/2 & \quad \text{on } DA
 \end{aligned} \tag{1}$$

as shown in Fig. 3, where  $u_x$ ,  $u_y$  are the displacement components in the  $x$ ,  $y$  directions, respectively, and  $t_x$ ,  $t_y$  are traction components in the  $x$ ,  $y$  directions. The additional constant  $C$  will be determined by an additional equilibrium condition :

$$\int_{BC} \mathbf{s}_y(x, a) dx = 0 . \quad (2)$$

For the purpose of determining the shear modulus, boundary conditions are given as:

$$\begin{aligned} u_y = 0 \quad t_x = 0 & \quad \text{on } AB \\ u_x = 1 \quad u_y = 0 & \quad \text{on } BC \\ u_y = 0 \quad t_x = 0 & \quad \text{on } CD \\ u_x = 0 \quad u_y = 0 & \quad \text{on } DA \end{aligned} \quad (3)$$

as shown in Fig. 4.

### **3. BEM Formulation**

Considering the unit cell as shown in Fig. 2(a), it is well known [5] that the Boundary Integral Equation (BIE) for the fiber can be written as

$$\frac{1}{2} u_j(p) = \int_{S_1} [u_i(q) T_{ij}(p, q) - t_i(q) U_{ij}(p, q)] ds(q) \quad (4)$$

where  $p$  as well as  $q$  are on  $S_1$ , see Fig. 2(a), the index  $i$  ( or  $j$  ) is equivalent to  $x, y$  when it varies from 1 to 2,  $u_i(q)$  are the displacements on the fiber side of the interface, and  $t_i(q)$  are the tractions exerted by the matrix on the fiber.  $T_{ij}, U_{ij}$  are fundamental tensors derived from the point-force solution of the elasticity equations for the plane strain problem [5]. The normal points away from the region of the fiber.

For the matrix, both  $S_1$  and  $S_2$ , see Fig. 2(a), form the boundary of this material. Thus for  $p$  and  $q$  on  $S_1$  and  $S_2$ , the BIE takes the form

$$\frac{1}{2}v_j(p) = \int_{S_1+S_2} [v_i(q)T_{ij}(p,q) - s_i(q)U_{ij}(p,q)]ds(q). \quad (5)$$

Again the normal points away from the region,  $v_i(q)$  are the displacements on the matrix boundary, and  $s_i(q)$  are the tractions by the fiber on the matrix.

In addition to these two BIEs, we need an interface condition because both displacements and tractions are unknown on the interface.

For a perfect interface between fiber and matrix, it is well known that the interface conditions are continuity of displacements and tractions across the interface, i.e.

$$\begin{aligned} u_i(q) - v_i(q) &= 0 \\ t_i(q) + s_i(q) &= 0. \end{aligned} \quad (6)$$

For an imperfect interface, the flexibly-bonded interface was chosen among many proposed interface models [6,10], to simulate the interface condition between the fiber and matrix. This interface model is in fact a ‘spring contact’ type which allows both slip and separation. It is assumed that the tractions are continuous across the interface, while the displacement may be discontinuous from fiber to matrix, and the displacement differences are linearly related to the conjugate tractions on the interface. The proportionality constants characterize the stiffness of the interphase. In mathematical form:

$$[t] = 0 \quad [u] = 2\mathbf{F}t \quad (7)$$

where square brackets denote discontinuities across the interface.

$$[t] = \begin{Bmatrix} t_s(q) + s_s(q) \\ t_n(q) + s_n(q) \end{Bmatrix} \quad (8)$$

$$[u] = \begin{Bmatrix} u_s(q) - v_s(q) \\ u_n(q) - v_n(q) \end{Bmatrix} \quad (9)$$

$$\mathbf{t} = \begin{Bmatrix} t_s(q) \\ t_n(q) \end{Bmatrix}. \quad (10)$$

$\mathbf{F}$  is called the flexibility matrix which has diagonal form

$$\mathbf{F} = \begin{bmatrix} M_s & 0 \\ 0 & M_n \end{bmatrix}$$

$$M_s = \frac{h}{\mathbf{m}} \quad M_n = \frac{h}{\mathbf{l} + 2\mathbf{m}} \quad \text{or} \quad \frac{h}{E}$$

where  $\mathbf{l}$  and  $\mathbf{m}$  are the Lamé moduli of a thin elastic layer of thickness  $h$  modeling the bond between the fiber and matrix. This include the limiting case of perfect bonding when  $\mathbf{m}$  is set to infinity or  $h$  is set to zero.

To avoid an unrealistic radial overlap of the two materials in the interfacial zone, when  $t_n(q) \leq 0$  we let

$$\begin{aligned} t_n(q) + s_n(q) &= 0 & u_n(q) &= v_n(q) \\ t_s(q) + s_s(q) &= 0 & u_s(q) - v_s(q) &= 2M_s t_s \end{aligned} \quad (13)$$

otherwise we use eqn (7).

Eqns (7) and (13) are in the local normal and tangential coordinate system. Assuming the normal at  $q$  is  $\bar{n} = (n_x, n_y) = (\cos \mathbf{a}, \sin \mathbf{a})$ , as shown in Fig. 5, the interface conditions in a global  $xy$  coordinate system are

$$\begin{Bmatrix} u_x - v_x \\ u_y - v_y \end{Bmatrix} = 2[T]^{-1} \begin{bmatrix} M_s & \\ & M_n \end{bmatrix} [T] \begin{Bmatrix} t_x \\ t_y \end{Bmatrix} \quad (14)$$

or in the region where radial overlap occurred

$$\begin{Bmatrix} u_x - v_x \\ u_y - v_y \end{Bmatrix} = 2[T]^{-1} \begin{bmatrix} M_s & \\ & 0 \end{bmatrix} [T] \begin{Bmatrix} t_x \\ t_y \end{Bmatrix}. \quad (15)$$

[T] is the coordinate transformation matrix

$$[T] = \begin{bmatrix} \sin \mathbf{a} & -\cos \mathbf{a} \\ \cos \mathbf{a} & \sin \mathbf{a} \end{bmatrix}. \quad (16)$$

These relations are sufficient to determine all boundary tractions  $t_i(q)$ ,  $s_i(q)$  and all boundary displacements  $u_i(q)$ ,  $v_i(q)$  at all points  $q$  on both  $S_1$  and  $S_2$  from a specification on the outer boundary  $S_2$ . Once all boundary functions are determined, the average tensile stress is calculated by

$$\overline{\mathbf{s}_x} = \frac{1}{2a} \int_{AB} \mathbf{s}_x(a, y) dy. \quad (17)$$

The effective tension modulus for the plane strain problem is obtained by

$$\begin{aligned} \overline{E_s} &= \frac{\overline{\mathbf{s}_x}}{\mathbf{e}_x} \\ \mathbf{n}_s &= -\frac{\mathbf{e}_y}{\mathbf{e}_x} = C \end{aligned} \quad (18)$$

where  $\mathbf{e}_x$  is the strain which can be evaluated from the prescribed boundary condition on edge  $AB$ .

In order to compare with analytical results, we need to calculate the intrinsic material properties from our plane strain numerical results. The relation between the material elastic moduli and the plain strain tension moduli is

$$\bar{E} = \frac{1 + 2\mathbf{n}_s}{(1 + \mathbf{n}_s)^2} \bar{E}_s . \quad (19)$$

The displacement components and stress components at any arbitrary interior point  $P$  of the fiber or the matrix can be obtained easily by the integral identity:

$$u_j(P) = \int_S [u_i(q)T_{ij}(P, q) - t_i(q)U_{ij}(P, q)] ds(q) . \quad (20)$$

The stresses at internal points are calculated by

$$\begin{aligned} \mathbf{s}_{ij} &= \mathbf{l} d_{ij} u_{l|l} + \mathbf{m} \left( \frac{\int u_i}{\int x_j} + \frac{\int u_j}{\int x_i} \right) \\ &= \int_S [D_{kij}(P, q)t_k(q) - S_{kij}(P, q)u_k(q)] ds(q) \end{aligned} \quad (21)$$

where the third order tensor components  $D_{kij}$  and  $S_{kij}$  correspond to derivatives of the fundamental solution [7]. In eqns (20) and (21)  $S$  is the boundary for the domain. For  $P$  inside the fiber,  $S = S_1$ , for  $P$  inside the matrix  $S = S_1 \cup S_2$ .

#### **4. Numerical Examples**

Numerical experiments were performed for several fiber/matrix combinations and fiber volume fractions to calculate the effective transverse tension modulus and shear modulus for fiber reinforced composites. Good agreements are obtained comparing our results with other numerical calculations and experimental data. Listed below are some typical examples using quadratic boundary elements. In our calculations for the entire unit cell model, a 96 element, 192 node mesh was used. For the one-quadrant model, similar results were obtained using a 40 element mesh.

The first example involves calculation of effective transverse tension modulus for a glass/epoxy composite material. The material constants are :

$$\text{for glass fiber} \quad E_f = 10.5 \times 10^6 \text{ psi} \quad \mathbf{n}_f = 0.22$$

$$\text{for epoxy resin matrix} \quad E_m = 0.5 \times 10^6 \text{ psi} \quad \mathbf{n}_m = 0.35 .$$

Calculations were performed for three volume fractions-- 19.63%, 45%, 60%. Our computed values of effective transverse moduli are plotted in Fig. 6. The solid line is the result obtained by the self-consistent cell model , the broken line is the result by Herman , the 'o' are the boundary element calculations made by N. Oshima [3]. Constant boundary elements were used in his calculations. It is seen that our results, indicated by '+' are in good agreement with all the results presented in Ref [3] as shown in Fig. 6.

Another example is calculated in order to compare our effective transverse tension modulus predictions with the Halpin-Tsai's equations and Finite Element Analysis calculations. Fig. 7 shows the present prediction for effective transverse tension modulus for various reinforcements/matrix stiffness ratios. The solid lines are the results of Adams and Doner's Finite Element Analysis [9] and the result from the Halpin-Tsai equations [8] are also presented in Fig. 7 by circles. We plot only our results for fiber volume fractions ( $V_f$ ) which are less than 70%. For composites with fiber volume fractions higher than 70%, nearly singular integrals, as a consequence of the proximity of boundary  $S_1$  and  $S_2$ , can causes unacceptable numerical errors. Although we can solve this problem to some extent by using smaller elements or higher order quadrature, we feel that this is not an effective way to deal with high fiber volume fraction composites. Instead we could use another basic cell model,

like the hexagonal unit cell or the equilateral triangle unit cell. Fortunately, however, for most fiber reinforced composite materials,  $V_f$  is less than 70%.

One more example is calculated for the perfect bonding interface to determine the transverse shear modulus for Kevlar/epoxy composites with 3 different fiber volume fractions. The calculated results are listed in Table. 1. The upper and lower bound solutions predicted by Hashin [12], by Teply and Dvorak [11] and by Yeh [2] (using finite element analysis) are also listed in the tables for comparison. It can be seen that our results are in good agreement with them. The present BEM result is slightly lower than the FEM result probably because the displacement based FEM usually gives a stiffer prediction than the exact value. The material constants used are :

Table 1 Transverse shear modulus (GPa) of Kevlar/epoxy composites

$V_f$	0.2	0.4	0.6
Hashin's model			
upper bound	1.313	1.571	1.872
lower bound	1.297	1.526	1.814
Teply and Dvorak's model			
upper bound	1.305	1.540	1.844
lower bound	1.280	1.506	1.799
Yeh's FEM calculation	1.297	1.529	1.82
Present BEM Calculation	1.294	1.513	1.798

for Kevlar fiber,  $E_f = 7.00 \text{ GPa}$      $n_f = 0.3$

for epoxy resin matrix,  $E_m = 3.00 \text{ GPa}$      $n_m = 0.35$ .

To study the effect of interface conditions on effective modulus and state of stress, the numerical calculations were carried out for carbon/epoxy composites. The material constants are :

for carbon fiber,  $E_f = 13.75 \text{ GPa}$      $n_f = 0.25$

for epoxy resin matrix,  $E_m = 1.862 \text{ GPa}$      $n_m = 0.33$ .

In the computation,  $M_n$  and  $M_s$  were taken as

$$M_n = \frac{h}{E} = \frac{k_2 b}{k_1 E_m} = k \frac{b}{E_m} \quad , \quad M_s = \frac{h}{\mathbf{m}} = \frac{k_2 b}{k_1 \mathbf{m}_m} = k \frac{b}{\mathbf{m}_m} \quad .$$

where  $b$  is the radius of the fiber. Five different values of  $k$ , 0, 0.1, 1, 10, 100 were considered. These values represent a decreasingly-stiff interphase with  $k = 0$  corresponding to a perfect bond. In the range of linear elasticity, the stress-strain curve is linear. Fig. 8 shows the stress-strain relations for the five values of  $k$ . As expected, the slope is steepest for a perfect bond, and the composite is stiffer for a stiffer interface.

The stress distribution for  $\mathbf{s}_x(a, y)$  for  $0 \leq y \leq a$  is also plotted in Fig. 9. This is the stress distribution in the matrix material along the edge  $AB$  of the unit cell. For a perfect bond, the largest  $\mathbf{s}_x$  occur at  $y = 0$  which is the middle of the edge  $AB$ . As the stiffness of the interface decrease substantially, the maximum stress moves to  $y = a$  which is the edge of the matrix, as can be seen for  $k=100$ . Thus for a perfect bond, the load is mainly carried by the fiber. As the interphase stiffness decreases, the load carried by matrix increases.

### ***5. A Library of Green's Functions***

In two of our previous papers [13,14], it has been shown that the main inverted coefficient matrix in any BEM may be regarded as a discretized Greens function which characterizes a material body and actually provides the solution for a specific boundary value problem. With such a matrix, a variety of boundary data, in the form of loads, incident waves, or other input data, which 'cause' a field of interest, are 'entered' as a column matrix. The desired field then is simply given by matrix multiplication with the mentioned inverted matrix or discretized Green's function.

For example, an elastodynamic scattering library has been formed and is used by physicists engaged in nondestructive evaluation at Iowa State University [15]. Entries in this library include inverted BEM matrices which characterize spheroidal voids in infinite elastic solids. These voids have a number of aspect ratios. The flatter ones are intended to simulate realistic open cracks, and various material properties are included, which pertain to commonly occurring solids used in aircraft. With this library, computer modelers easily impinge the various voids with elastodynamic waves of their choice, and pick up the scattered signal at desired locations. This is done making no meshes, no waiting for the solutions of large systems of equations, and indeed with no real knowledge of BEM codes or modeling strategy. All that is required is to enter chosen incident waves, and specify scattered wave locations, in an easy pre-specified format. Scattered signals are output in only the amount of time needed to multiply a square matrix by a column matrix and a row-times-column multiplication. Physical experiments have been modeled and 'what-if' numerical experiments may be

conducted, with negligible time and effort, using the library for common void scatterers in common materials.

What we are suggesting here is to form a similar library of Greens functions, with similar advantages, for the use by composite material community.

For example, for fiber reinforced composites, library entries could be based on any of, or any combination of, the following factors:

1. Various Fiber Volume Fractions
2. Various Constituent Stiffness Ratios  $E_f/E_m$
3. Different Interface Conditions
4. Amount of Debonding Around the Interface Perimeter

Library entries based on other criteria could be created, but all such entries should be chosen in the interest of and in consultation with the composites community.

The first entries probably should reflect the most-needed and most-often-used parameters, in present use, and in proposed design of new materials. Again, the goals are easy and quick numerical simulations for calculating such things as effective moduli and peak interface stresses. Simulating the effects of the most common types of damage expected, with existing and new materials, should be especially welcome. Simulating the effects of thicknesses of fiber coatings, and thus the response characteristics of various interface conditions should be welcome as well. The main point is that all modeling, with the Library in hand, could be done by composites workers who need not necessarily be experts in any kind of computer modeling.

Other BEM libraries, for elastostatic analysis as needed by design community, are also being constructed at Iowa State University. All such libraries benefit from cooperation between BEM researchers and industry or researchers in other areas.

### ***Acknowledgment***

Portions of this work have been supported by the National Science Foundation and the National Institute of Standards and Technology with the cooperation of the Colorado School of Mines under contract # 4-41578. Thanks are also due the AEEM Department and College of Engineering of Iowa State University for additional support.

### ***References***

1. D. F. Adams. A Micromechanics Analysis of the Influence of the Interface on the Performance of Polymer-Matrix Composites. *Journal of Reinforced Plastics and Composites*, Vol. 6, 66-88, (1987).
2. J. R. Yeh. The Effect of Interface on the Transverse Properties of Composites. *Int. J. Solids Structures*, Vol. 29, 2493-2505, (1992).
3. N. Oshima and N. Watari. Calculation of Effective Elastic Moduli of Composite Materials with Dispersed Parallel Fibers. *Theoretical and Applied Mechanics*, Tokyo University Press, Vol. 41, 181-188, (1992).
4. J. D. Achenbach and H. Zhu. Effect of Interfacial Zone on Mechanical Behavior and Failure of Fiber-Reinforced Composites. *J. Mech. Phys. Solids*, Vol. 37 (3), 381-393, (1989).

5. F. J. Rizzo and D. J. Shippy. A Formulation and Solution Procedure for the General Non-Homogeneous Elastic Inclusion Problem. *Int. J. Solids Structures*, Vol. 4, 1161-1179, (1968).
6. P. A. Martin. Boundary Integral Equations For the Scattering of Elastic Waves by Elastic Inclusions with Thin Interface Layers. Preprint.
7. C. A. Brebbia and J. Domiguez. *Boundary Element, an Introductory Course*. Computational Mechanics Publications, Southampton, U.K., (1989).
8. J. C. Halpin and S. W. Tsai. Effects of Environmental Factors on Composite Materials. AFML-TR 67-423, (1969).
9. D. F. Adams and D. R. Doner. Transverse Normal Loading of a Unidirectional Composite. *J. Composite Materials*, Vol. 1, 152-163, (1967).
10. Z. Hashin. Composite Materials with Interphase: Thermoelastic and Inelastic Effects. *Inelastic deformation of Composite Materials*, G. J. Dvorak, ed. Springer, New York, 3-34, (1991).
11. J. L. Teply and G. J. Dvorak. Bounds on Overall Instantaneous Properties of Elastic-Plastic Composites. *J. Mech. Phys. Solids*, Vol. 36, 29-58 (1988).
12. Z. Hashin. Analysis of Properties of Fiber Composites with Anisotropic Constituents. *J. Appl. Mech.* , Vol. 46, 543-550, (1979).
13. P. A. Martin and F. J. Rizzo. Partitioning, Boundary Integral Equations, and Exact Green's Functions. *Int. J. Numer. Methods Eng.*, Vol. 38, 3483-3495, (1995).
14. F. J. Rizzo, P.A. Martin, L. Pan and D. Zhang. Exact Green's Functions and the Boundary Element Method. BEM 17, 17-19 July, (1995).

15. L. Pan. EWAS Scattering Library User's Manual. AEEM Dept., Report, Iowa State University, (1994).





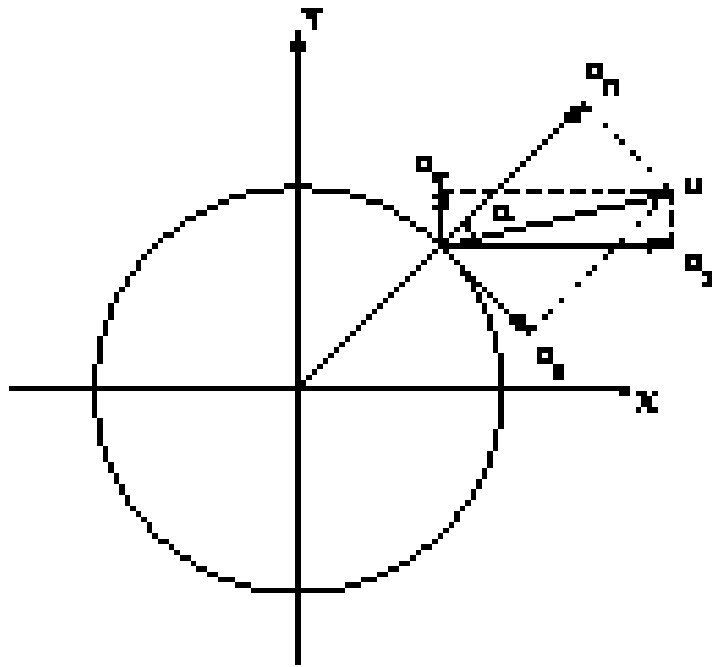


Fig. 5 Transformation between local sn and global xy coordinate system

Fig. 6.  $E_{\text{eff}}/E_m$  vs. the volume fraction  $V_f$  (From Ref. [3])

Fig. 7.  $E_{\text{eff}}/E_m$  vs.  $E_f/E_m$  (From Ref. [9])

Fig. 8. Stress-strain curves for different  $k$

Fig. 9 Matrix stress distribution along edge AB( $x = a$ )

**CHAPTER 3**

**SOME EFFICIENT BOUNDARY INTEGRAL STRATEGIES**

**FOR WAVE PROBLEMS IN AN ELASTIC HALFSPACE**

A paper submitted to the journal

Computer Methods in Applied Mechanics and Engineering

Lingyun Pan and Frank Rizzo

Department of Aerospace Engineering and Engineering Mechanics,

Iowa State University, Ames IA 50011, USA

P. A. Martin

Department of Mathematics

University of Manchester, Manchester M13 9PL, UK

***Abstract***

When Boundary Integral Equation/ Boundary Element Methods (BIE/BEMs) are used for halfspace problems, such as occur frequently in elastodynamics, the fullspace (Stokes) fundamental solution or halfspace (Lamb) fundamental solution can be used to formulate the BIE. When the fullspace fundamental solution is used, a truncated discretized model of the halfspace surface is required. Alternatively, if the halfspace fundamental solution which models the entire halfspace surface analytically is used, no truncation issues arise.

Nevertheless, both Stokes and Lamb approaches have advantages and disadvantages. This paper presents systematic strategies, based on the BEM for 3D halfspace elastodynamic problems, wherein the best features of formulations based on the Stokes and the Lamb solutions are exploited. Strategies are illustrated and numerical results are given for point sources and radiation from a spherical void in a halfspace.

## ***1. Introduction***

Boundary Integral Equation/Boundary Element Methods (BIE/BEMs) have proven to be powerful tools for formulating and numerically attacking exterior boundary value problems. In this paper the BIE method refers to the formulation of a problem in terms of integral equations defined on the boundaries of a domain. The BEM refers to the procedure used to discretize the integral equations, using boundary elements, and the procedure used to solve the integral equations numerically. These tools have certain advantages over domain-based numerical methods for such problems. With the (radiation) conditions on the surface at infinity incorporated analytically, only finite surface(s) need to be discretized when the only other surface(s) in the problem are finite in extent. With domain-based numerical methods, such as the finite element method, element-modeling of an entire infinite domain is, of course, impossible. Simply truncating the finite-element model of the infinite domain is usually inadequate. Thus, special features are introduced into these methods to model such a domain and to satisfy the radiation condition [1].

However, when a BEM is used for halfspace problems, such as occur frequently in elastodynamics, and the fullspace (Stokes) fundamental solution is used to formulate the BIE, a truncated discretized model of the halfspace *surface* is required. (Usually, a discretized

model of a finite surface, such as a buried finite obstacle, is needed as well). Therefore, a truncation problem can exist in modeling a halfspace problem, even with boundary methods. However, with Stokes and the BEM, the truncation issue is different than with say finite elements. With finite elements the domain itself and not just a bounding surface must be truncated; thus the nature of each kind of truncation is different in a very basic way. Indeed, a good boundary solution can usually be obtained with the BEM even with severe truncation of the halfspace surface. This truncation may be simple, i.e., no special layer of ‘infinite’ elements to simulate the ‘rest of the halfspace surface’ need be used.

Alternatively, if the BEM procedure uses the Lamb fundamental solution, which models the complete halfspace surface analytically, no truncation issues even arise. But, since Lamb’s solution is available in an analytical form which requires (numerical) evaluation of infinite integrals with respect to frequency, the CPU time spent on just forming a boundary integral equation is increased significantly and often prohibitively. Further, for some combination of locations of source point and field point, it is especially difficult or, with certain algorithms, impossible to evaluate the Lamb solution.

Problems of radiation and scattering in a halfspace have been under investigation via BIE/BEM for some time. In the time domain, the BIE has been used for halfspace dynamics problems [2,3] for linear and nonlinear problems. In both studies, the Stokes solution was employed, and discretization over the halfspace surface was required. In the frequency domain, the BIE was used for the foundation problems in a halfspace [4] for studying the dynamic response of rectangular foundations. Again, the Stokes solution was used, and a truncation on the halfspace surface was needed. However, in [5] and [6] the Lamb solution

was used to formulate the axisymmetric BIE for a layered viscoelastic halfspace to avoid discretization of the halfspace surface. A BIE formulation using Lamb's solution for elastic halfspace problems, free from principal-value integrals, was proposed in [7]. In a follow-up study [8], halfspace problems were considered by BIE formulations using both Stokes' and Lamb's tensors. Comparisons were done by checking boundary solutions obtained with both kernels. However, truncation effects on the boundary solution, as well as on the solution for interior points were not addressed.

In summary, all of the researchers cited above attacked the halfspace problem by the BIE either by using the Stokes solution, making a truncated discretization on the halfspace surface, getting a fairly good solution on the boundary, or by using the Lamb solution without concern for computational efficiency. Several questions arise then regarding the BEM for halfspace problems; such as, can good results be obtained everywhere by using the Stokes solution alone? Is it always better to just use the BIE formulation using the Lamb solution? Is there a way to take advantage of both formulations to attack halfspace problems if questions of practicality and efficiency must govern? An attempt is made to answer these questions in this paper.

Specifically, we present systematic strategies, based on the BEM for halfspace elastodynamic problems, wherein the best features of the Stokes solution and the Lamb's solution are exploited. This research is motivated by a general class of problems related to responses due to explosions or other disturbances inside an underground structure. Here we restrict ourselves to time-harmonic radiation problems, even though we can study scattering

problems in a similar manner and can deal with transient problems through the Fourier transform and the Laplace transform [9].

Most of our strategies are illustrated and numerical results are presented for point sources in a halfspace and radiation from a spherical void in a halfspace.

## ***2. BIE Formulations***

Consider a homogeneous, isotropic, elastic halfspace bounded by a flat halfspace surface  $S_H$  at  $z=0$ , which is traction free, as shown in Figure 1. The elastic material fills the halfspace  $z \geq 0$ . There is a finite obstacle  $B$  inside the halfspace with a surface  $S_2$ . In the region  $B'$ , exterior to  $B$  but within the halfspace, we assume that an elastic field exists in the form of a time harmonic displacement vector  $u_i(p, \mathbf{w})$ , which must satisfy the familiar Navier equation,

$$(c_1^2 - c_2^2)u_{j,ji} + c_2^2 u_{i,jj} + \mathbf{w}^2 u_i = 0 \quad (1)$$

where  $c_1$  and  $c_2$  are dilatational- and shear-wave speeds, respectively,  $\mathbf{w}$  is the circular frequency, and body forces are assumed to be zero. This field is assumed to arise from a prescription of boundary data on  $S_2$

Next, a Somigliana integral formula based on the Stokes point force solution may be derived ( see [7]), and written as:

$$C_{ij}(p)u_j(p) = \int_{S_H+S_2} \left[ T_{ij}(p,q)u_j(q) - U_{ij}(p,q)t_j(q) \right] ds(q) \quad (2)$$

in which  $U_{ij}$  and  $T_{ij}$  are Stokes' displacement and traction tensors, respectively, which describe the fields at a point  $q$  due to a time harmonic point force of frequency  $\mathbf{w}$  at a point  $p$  in a

fullspace [7]. Here we assume no incident wave in  $B'$  and  $C_{ij}(p)$  is the coefficient tensor of the free term (again see [7]) and is a function of the location of  $p$ . When  $p$  is inside  $B'$ , eqn. (2) is a representation integral which gives the solution at  $p$  in terms of boundary values of  $u_j(q), t_j(q)$  on both  $S_H$  and  $S_2$ , and  $C_{ij}(p) = \mathbf{d}_{ij}$ . When  $p$  is on the boundary, either  $S_H$  or  $S_2$ , eqn. (2) is a BIE in which half of the pair of variables  $u_j(q), t_j(q)$  are prescribed for a well-posed problem. The BIE (2) can be solved for the other half of the boundary data.

Indeed, in the BIE process, the first step is to put  $p$  on the boundary; the BIE is then solved for the unknown boundary data. In the second step, the solution at any point inside the domain  $B'$  can be obtained from the representation integral. In both steps, all of the integrals are evaluated numerically, so a discretization is needed on both the halfspace surface and the finite surface. Since  $S_H$  is infinite, only a truncated finite area  $S_1$  would be discretized. Thus truncation arises when solving the BIE as well as when obtaining the solution at a field point.

Denote the neglected area on the halfspace surface as  $S_\infty$  (see, Figure 1), i.e.

$S_H = S_1 \cup S_\infty$ , and for all problems of interest in this paper,  $t_j(q) \equiv 0$  on  $S_H$ . Thus, the BIE eqn. (2) can be expanded as:

$$C_{ij}(p)u_j(p) = \int_{S_2} [T_{ij}(p, q)u_j(q) - U_{ij}(p, q)t_j(q)] ds(q) + \int_{S_1} T_{ij}(p, q)u_j(q) ds(q) + \int_{S_\infty} T_{ij}(p, q)u_j(q) ds(q). \quad (3)$$

The last term is associated with the neglected area  $S_\infty$ . For  $p$  located on  $S_2$  or  $S_1$ , and  $q$  on  $S_\infty$ , we find that the contribution of this last term may be neglected without detriment to the

accuracy of the boundary solution, provided  $S_1$  has at least a minimum size. This matter is discussed in some detail in the next section.

Now if instead of the Stokes tensor  $U_{ij}$  and  $T_{ij}$ , Lamb's tensors  $U_{ij}^H$  and  $T_{ij}^H$  are used, the Somigliana integral need only be taken over  $S_2$  because the presence of the traction-free halfspace surface is accounted for in Lamb's tensors. That is,  $T_{ij}^H(p, q) = 0$ , whenever  $q$  is on  $S_H$  ( see [14] ). Thus, the Somigliana integral formula has the simple form:

$$C_{ij}(p)u_j(p) = \int_{S_2} \left[ T_{ij}^H(p, q)u_j(q) - U_{ij}^H(p, q)t_j(q) \right] ds(q) . \quad (4)$$

There is no truncation issue because the integral is taken only over the finite surface  $S_2$ . However, the computation of Lamb's halfspace Green's function for (4) as a BIE is very time consuming. To give an idea of the CPU time difference between formulating and solving the BIE using the Stokes solution, and formulating and solving the BIE again using the Lamb solution, an experiment was performed for a sphere, in a fullspace, with an 8 element discretization. It took 2.8 seconds to solve the BIE using the Stokes solution. When the Lamb solution was used, the CPU time was 820 seconds. Thus we were motivated to look carefully at the Stokes formulation despite the shortcomings, conceptually at least, of truncation.

### ***3. Truncation Study for the BIE Using the Stokes Solution***

To investigate truncation effects on boundary solutions and results at field points via Stokes, the problem of a point load in a halfspace was considered first. Displacements on the halfspace surface obtained as the boundary solution in the Stokes BIE should then be identical

to the corresponding displacements given by the halfspace Green's function  $U_{ij}^H$ . Because of the absence of  $S_2$  and the existence of the point source, the Stokes BIE (3) reduces to:

$$C_{ij}(p)u_j(p) = \int_{S_1} \left[ T_{ij}(p,q)u_j(q) - U_{ij}(p,q)t_j(q) \right] ds(q) + U_{ij}(p,p_0)F_j(p_0) \quad (5)$$

in which  $p_0$  is the location of the point source;  $F_j$  is the magnitude or strength vector of the point source.

The point source is one unit below the halfspace surface, and is in the  $z$  direction for all the results presented here. This makes  $F_1 = F_2 = 0$ ,  $F_3 = 1$  in eqn. (5). In Figure 2, we show the comparison between our boundary solutions and exact point force solutions for the magnitude and phase angle of  $u_1$  and  $u_3$  components along  $x$  direction on the halfspace surface. The results presented there are for a point source in titanium alloy ( $c_1 = 6340 \text{ m/s}$ ,  $c_2 = 3030 \text{ m/s}$ , Poisson's ratio  $\nu=0.352$ .) when the discretized area  $S_1$  is chosen as a  $12 \times 12$  square area. (Later we will show that a much smaller discretized area  $S_1$  can be used to obtain a good solution). The shear wave number is  $k_t=0.449$ , The discontinuity in the phase-angle plot is caused by the jump in  $+180^\circ/-180^\circ$ . Note that the validity of our BEM analysis is confirmed by the good agreement between our computed results and that given by the analytical solution  $U_{ij}^H$ .

In Figure 3, we show the variation of the magnitude of scattered field  $u_3$  along the  $x$  direction for four different sizes of the discretized area  $2L \times 2L$  of  $L=3, 4, 6, 12$  respectively, over the halfspace surface. It is seen that the results converge very well. Very good results can be obtained by using a relatively small discretization ( $L=3$ ). The main effect of a larger discretization is to obtain some extension of the curve over the added-discretized portion of

$S_H$ . That is, the increase in accuracy of the boundary values of  $u_3$  over a given discretized model of  $S_H$ , by making that model larger, seems to be small.

Observations made about data from point source results are very important because the radiation from any kind of a shape in the halfspace could be viewed as the radiation by a distribution of point sources. To confirm this, we studied the radiation from a spherical void which is used to simulate a spherical wave in the halfspace.

Consider a spherical cavity of radius  $r$  which is buried at a distance  $d$  inside a homogeneous, elastic half-space and which is radiating harmonic dilatational waves into the halfspace, such that  $t_r = 1.0$ ,  $t_q = t_f = 0.0$ .

Since the magnitude of spherical waves decreases with distance from the source, the reflected waves due to the presence of the halfspace surface also have a diminishing effect as they travel through the medium. Thus, it is expected as the distance  $d$  increases, the surface data on the sphere should approach the corresponding fullspace solution. This observation can be viewed as a check for the algorithm and coding (analytical comparison data are not available for this problem), and the expected behavior is apparent from Figure 4, in which the polar variation of the boundary solutions on plane  $y = 0$  for several different depth of the sphere when  $k_p r = 0.913$  ( $k_p$  is the dilatational wave number), poisson's ratio  $\nu = 0.25$  are plotted. It can be seen when  $d \geq 8r$ , the surface data are quite close to the corresponding fullspace solution.

Figure 5 shows the variation of  $u_1$  and  $u_3$  components on the halfspace surface obtained using three different sizes of discretization  $2L \times 2L$  on the  $S_H$  surface. It is again very

clear that we pick up more information as we increase the size of the discretization. However, values of new data compared with values of previously-obtained data again show little change.

The situation for interior points is, however, different. Calculation for  $u_1$  and  $u_3$  at various locations of interior points, for the largest discretization of  $S_H$ , were performed and compared to the analytical solution for point load case. The general conclusion, for interior points, is that we can obtain good results for points only under the “shadow” of the halfspace discretization. Figure 6 shows the result for interior points one unit below the halfspace surface from  $x = 2$  to  $x = 25$  due to the point load in the halfspace. It can be seen that beyond  $x = 10$  the result from BEM deviates considerably from the Lamb solution.

Therefore, while we can obtain very satisfactory boundary data over the discretized surfaces with reasonable truncation of  $S_H$ , via the Stokes BIE, we can not obtain satisfactory field data at distances much beyond the edge of the truncated  $S_H$ . It is obviously impractical to use ever-larger models of  $S_H$  just to get desired field data at large distances from the sources of disturbance. Thus, what can be done?

#### ***4. Lamb's Formulation Revisited***

We mentioned earlier that using the Lamb solution in forming and solving a BIE would be prohibitive for any problem requiring a substantial amount of discretization over  $S_2$  because of the CPU time involved to get function evaluations for the many  $p$ -Gaussian quadrature point combinations involved. Note, we speak of prohibitive CPU time despite the fact that discretization of (a portion of)  $S_H$  is not even an issue with Lamb. However, suppose we get good boundary displacements over  $S_2$  with a fairly small discretization

(reasonable truncation) of  $S_H$ , as we have shown that we can do. Then if we ask for field data, remote from  $S_2$ , via eqn. (4) used as a representation integral for comparatively *few* points  $p$ , the costs are very reasonable indeed. In fact, we may view this as an ideal compromise, the best of both worlds in a sense: specifically, use Stokes, with a reasonable truncation of  $S_H$ , to form and solve the relevant BIE; thus obtain  $u_j(p)$  on  $S_2$  accordingly, efficiently, and in reasonable time; then use Lamb in the representation integral to get the farfield data which requires boundary data over  $S_2$  only. A similar strategy was used in [15] for scattering from a halfspace surface-breaking crack problem.

Figure 7 shows the interior results calculated by using Stokes in the BIE and using Lamb in the representation integral (indicated by +) compared with the results from using Lamb's solution in both the BIE and the representation integral. Also in Figure 7 is the uncorrected results if Stokes is used both in the BIE and in the representation integral. It is very obvious that those uncorrected results denoted by circles deviate from the good results even for field points which are close to the origin.

### ***5. A More Efficient and Faster Strategy: the Library***

The efficiency of using the Stokes-plus-Lamb strategy described above can be improved by incorporating the idea of a 'Green's function Library' ( see [11,12] ). For problems with two surfaces as the boundary, such as halfspace problems ( $S_2$  plus  $S_H$ ), a sub-matrix of the coefficient matrix is the essential part of the partial Green's function for the problem. The library idea is closely related to partitioning of the system matrix.

The BIE in discretized form for the halfspace problem, using the Stokes tensors, can be written as:

$$\begin{bmatrix} A_{11} & A_{12} \\ A_{21} & A_{22} \end{bmatrix} \begin{Bmatrix} u_1 \\ u_2 \end{Bmatrix} = \begin{Bmatrix} f_1 \\ f_2 \end{Bmatrix}$$

where  $A_{11}$  are coefficients related to collocation(source point  $p$ ) on  $S_1$ , and integration (integration point  $q$ ) on  $S_1$ ;  $A_{12}$  are coefficients related to collocation on  $S_1$  and integration on  $S_2$ ;  $A_{21}$  are coefficients associated to collocation on  $S_2$  and integration on  $S_1$ ;  $A_{22}$  are coefficients associated to collocation on  $S_2$  and integration on  $S_2$ ; In the recent papers[11,12], it has been shown that  $A_{11}^{-1}$  is in fact the essential ingredient in a ‘discretized Green’s function’ for the halfspace problem.

Indeed, suppose we attempt to solve this system of equations via partitioning, i.e. form  $A_{12}$ ,  $A_{21}$ , and  $A_{22}$  and write the following reduced system of equations:

$$(A_{22} - A_{21}A_{11}^{-1}A_{12})\{u_2\} = \{f_2 - A_{21}A_{11}^{-1}f_1\}. \quad (7)$$

Then obtain  $u_1$  by

$$\{u_1\} = A_{11}^{-1}\{f_1 - A_{12}u_2\}. \quad (8)$$

Suppose further that the discretization on the halfspace surface is bigger than the discretization on the finite surface. The size of  $A_{11}$  is then much bigger than the size of  $A_{22}$ . The most computationally intensive part of the solution via eqns (7) and (8) then is the formation and inversion of  $A_{11}$ . This leads to the idea of making an accurate discretization of the halfspace surface, obtaining  $A_{11}^{-1}$ , and storing this large matrix so that it can be reused over and over again with different  $S_2$ . This idea is becoming attractive as storage and retrieval of mass-amounts of data become easier and cheaper. Also only the boundary data on  $S_2$  is of

interest when using Lamb. Thus, we do not really need to go through eqn. (8) to get  $u_1$ . In actual implementation, the matrix saved is not the inverse of  $A_{11}$ , but the LU decomposition of  $A_{11}$ .

As an illustration of the benefits of this partitioning-library strategy, Table 1 shows some CPU times for a typical halfspace problem solved in two ways. It can be seen that by doing partitioning, the CPU time is approximately 1/10 of the CPU time needed for solving the whole problem in one step.

### ***6. Some Useful Approximations***

Some useful approximations might be appropriate for the halfspace problem. First, if the finite obstacle is deep enough below the halfspace surface, we can approximate the boundary solution on the surface of the finite obstacle by solving a fullspace problem,

Table 1 CPU time comparison for partitioning using Library idea

Method/Task	CPU time (seconds)
CPU time for solving the problem in one step 144 elements on the halfspace surface, 8 elements on the sphere	1920
CPU time via Partitioning	
Form $A_{11}$	870
LU decomposition	866
Pre-effort (form $A_{11}$ and save LU decomposition of $A_{11}$ )	1636
Form $A_{22}, A_{21}, A_{12}$	70
read LU decomposition of $A_{11}$	7.8
Calculate new coefficient matrix and right hand side	95.5
Solve the reduced equations	0.05
Total CPU time for partitioning	173

and then this approximation gives very good results. Figure 8 shows the interior results calculated in this way for  $d=8r$  compared with the results from using Lamb's solution. This approximation gives good results for both the magnitude and the phase angle even for farfield points. Further, we found that certain asymptotic techniques for special locations of the field points are often warranted. For example, we found that the scattered field on the halfspace surface exhibits very good Rayleigh wave features when the distance from the origin gets large. This can be seen from Figure 9 in which the scattered field on the halfspace surface is plotted. The two main characteristics of the Rayleigh wave, i.e. the magnitude of the displacement decays very slowly and a  $90^\circ$  phase angle difference exists between  $u_1$  and  $u_3$ , are very apparent. For the field caused by the radiation from a spherical void, even though the Rayleigh wave is not evident in the near field, it is found that, at certain larger distance from the origin, the scattered field also exhibits the Rayleigh wave characteristics. Thus, if the major part of the field on the halfspace surface comes from the Rayleigh wave for large distance from the origin, it is possible to use the Rayleigh wave representation and boundary solutions from the BIE to approximate the farfield on the surface. However, specific strategies for using the boundary data from BEM to construct an appropriate Rayleigh wave representation is itself an interesting topic for future research.

## ***7. Conclusions***

Both BIE formulations, i.e. via Stokes' and Lamb's solutions, are used to attack halfspace problems, and compared with each other. Each has its own advantages and disadvantages.

It is found that when Stokes is used, the halfspace-surface truncation affects both the boundary solution and the solution at field points. However, it is also found that this truncation has a small effect on the boundary values themselves, i.e., very good boundary solutions can be obtained with a small size of discretization on the halfspace surface. On the other hand, the truncation has a big effect on the results for field points, especially those field points which are out of the "shadow" of the halfspace surface discretization. This is true even though important ingredients in the remote field point values are the truncation-insensitive boundary values. It is also found that when Lamb is used, the CPU times are usually prohibitive.

In this paper then, to counter the negative effects of truncation with Stokes and to address the excessive CPU issue with Lamb, we suggest the following: use Stokes to formulate the BIE and obtain good boundary solutions over the truncated halfspace plus a finite surface; then use Lamb's solution in the representation integral to evaluate results at field points. In this way, there are no adverse truncation effects on the results for field points, since the boundary solution on the finite surface is good, as stated, and the finite surface is the only one which must be integrated over with Lamb. For the relatively few function evaluations of Lamb's solution required in getting field point values only, CPU time is seldom a problem.

We also suggest that when using the fullspace fundamental solution in the BIE, considerable time and effort can be saved by pre-computing the coefficient matrix for the truncated halfspace surface model and storing its inverse (in reality the LU decomposition of that coefficient matrix) for repeated use. The Green's function Library idea, with the coefficient matrix for a fine discretization on the halfspace surface which is identified as the main ingredient of the partial Green's function, precomputed and stored, gives an even more efficient and faster way to attack halfspace problems.

Further, we found that certain approximations are applicable for the halfspace problem. For example, when the finite surface  $S_2$  is deep enough below the halfspace surface, we can approximate the boundary solution on the surface of  $S_2$  by solving a fullspace problem, and then obtaining the field in the halfspace by using Lamb's solution. Also some asymptotic techniques for special locations of the field points are often warranted. For example, if the major part of the field on the halfspace surface comes from the Rayleigh wave, we can use the Rayleigh wave representation and boundary solutions from the BIE to approximate the farfield on the surface.

### *Acknowledgment*

Thanks are due the Sandia National Laboratories, in Albuquerque, NM, for several communications which motivated some of this research. Many thanks are due also to Ron Roberts of the Center for Nondestructive Evaluation of Iowa State University for providing the code for calculating halfspace Green's functions and for many helpful discussions during all the phases of this project.

Finally, the authors are grateful to the Center for Computational and Theoretical Material Science of the National Institute for Standards and Technology, Gaithersburg, MD, for financial support of a portion of this research under grant No. 60NANB6D0210.

### *References*

1. D. Givoli, Numerical Methods for Problems in Infinite Domains(Elsevier, Amsterdam, 1992).
2. D.L. Karabalis, D.E. Beskos, Dynamic response of 3-D embedded foundations by the boundary element method, *Comp. Meth. Appl. Mech. Engrg.*, 56 (1986), 91-120.
3. S. Ahmad, Linear and nonlinear dynamic analysis by boundary element method, Ph.D. Dissertation, Dept. of Civil Engrg., SUNY at Buffalo, 1986.
4. J. Dominguez, Dynamic stiffness of rectangular foundations, Research Report R78-20, Dept. of Civil Engrg., Massachusetts Institute of Technology, Cambridge, Massachusetts, 1978.
5. R.J. Apsel, J.E. Luco, Impedance functions for foundations embedded in a layered medium: an integral equation approach, *Earthquake Engrg. Struct. Dynam.*, 15 (1987), 213-231.
6. F. Chapel, Boundary element method applied to linear soil structure interaction on a heterogeneous soil, *Earthquake Engrg. Struct. Dynam.*, 15 (1987), 815-829.
7. F.J. Rizzo, D.J. Shippy and M. Rezayat, A boundary integral equation method for time-harmonic radiation and scattering in an elastic half-space, in T.A. Cruse, A.B. Pifko, H. Arman eds., *Advanced Topics in Boundary Element Analysis, AMD-Vol. 72* (ASME, New York, N.Y.) 1985, 83-90.

8. I.R. Gonsalves, D.J. Shippy and F.J. Rizzo, Direct boundary integral equations for elastodynamics in 3-D half-spaces, *Computational Mechanics*, 6 (1990), 279-292.
9. M. Rezayat, D.J. Shippy and F.J. Rizzo, On time-harmonic elastic-wave analysis by the boundary element method for moderate to high frequencies, *Comp. Meth. Appl. Mech. Engrg.*, 55 (1986), 349-367.
10. F.J. Rizzo, D.J. Shippy and M. Rezayat, A boundary integral equation method for time-harmonic radiation and scattering of elastic waves in three dimensions, *Int. J. Num. Meth. Engrg.*, 21 (1985), 115-129.
11. P.A. Martin, F.J. Rizzo, Partitioning, boundary integral equations, and exact Green's functions, *Int. J. Num. Meth. Engrg.*, 38 (1995), 3483-3495.
12. F.J. Rizzo, P.A. Martin, L. Pan and D. Zhang. Exact Green's Functions and the Boundary Element Method, BEM 17, 17-19 July, (1995).
13. R.A. Roberts, Elastodynamic response of contacting fluid and solid half-spaces to a three-dimensional point load, *Wave Motion*, 12 (1990), 583-593.
14. K. Aki and P.G. Richards, *Quantitative Seismology*, Vols. 1,2 (W.H. Freeman, San Francisco, 1980).
15. D.E. Budreck and J.D. Achenbach, Three-dimensional elastic wave scattering by surface-breaking cracks. *J. Acoust. Soc. Am.* 86(1) (1989), 395-406.

$$S_H = S_1 \cup S_\infty$$

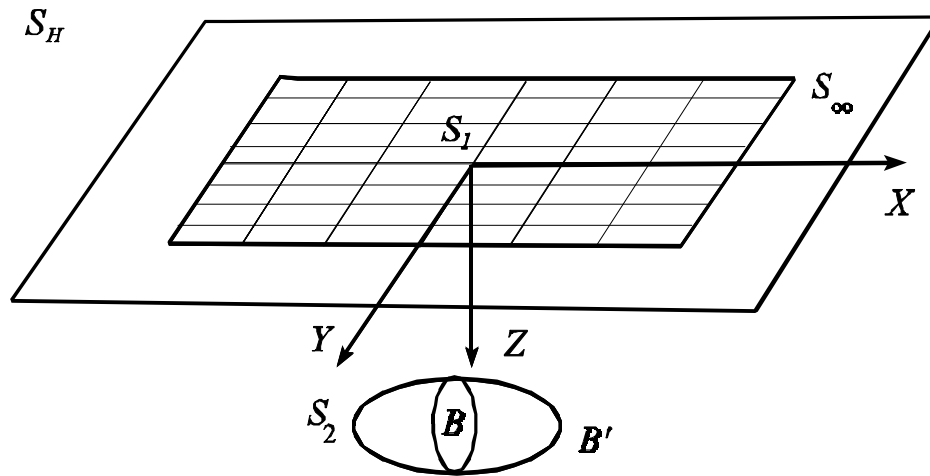


Figure 1 The halfspace problem

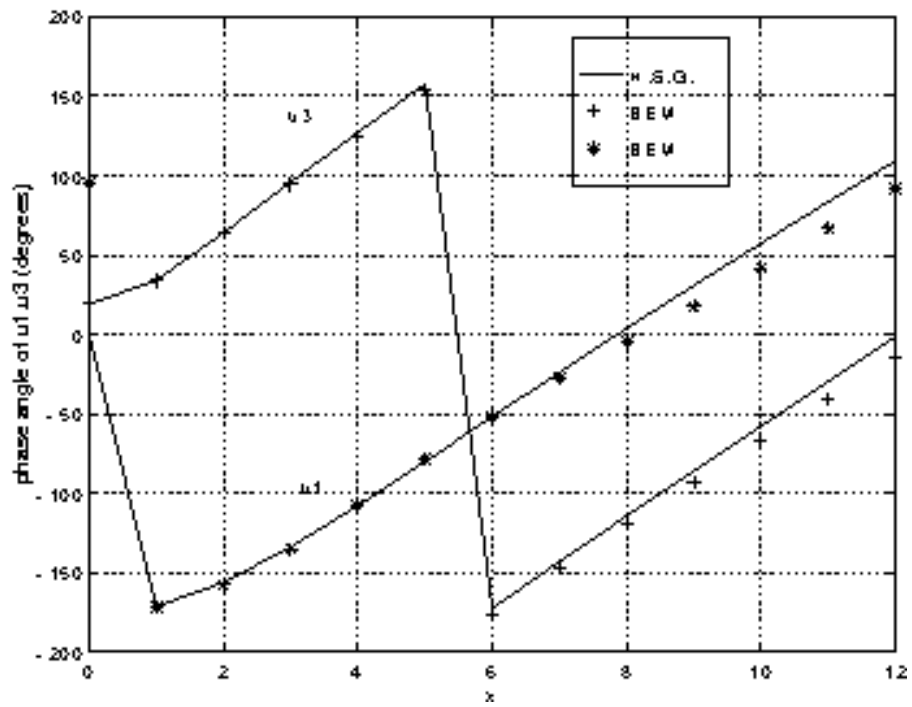


Figure 2 Comparison of boundary solutions from  $L=12$  discretization with Lamb's solution for point loading ( $d=1$ )

Figure 3 Truncation effect of point source response

Figure 4 Depth test for radiation from spherical void

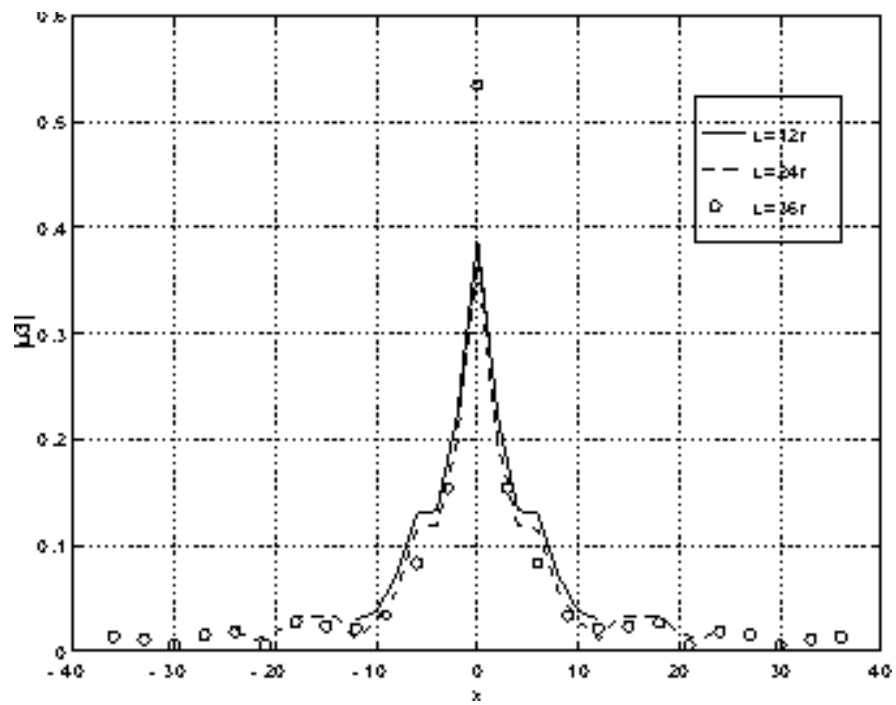


Figure 5 Truncation effect for radiation from a spherical void

Figure 6 Field values at interior points (point load)

Figure 7 Results from strategy proposed in this paper for interior points

Figure 8 Results by using large depth approximation

Figure 9 Rayleigh wave features for field due to point loading

CHAPTER 3 SOME EFFICIENT BOUNDARY INTEGRAL  
STRATEGIES FOR WAVE PROBLEMS IN AN ELASTIC HALFSPACE

.....	53
Abstract.....	53
1. Introduction.....	54
2. BIE Formulations.....	57
3. Truncation Study for the BIE Using the Stokes Solution.....	59
4. Lamb's Formulation Revisited.....	62
5. A More Efficient and Faster Strategy: the Library.....	63
6. Some Useful Approximations.....	65
7. Conclusions .....	67
Acknowledgment.....	68
References .....	69

Figure 1	The halfspace problem.....	71
Figure 2	Comparison of boundary solutions from $L=12$ discretization with Lamb's solution for point loading ( $d=1$ ) .....	72
Figure 3	Truncation effect of point source response .....	73
Figure 4	Depth test for radiation from spherical void.....	74
Figure 5	Truncation effect for radiation from a spherical void .....	75
Figure 6	Field values at interior points (point load).....	76
Figure 7	Results from strategy proposed in this paper for interior points.....	77
Figure 8	Results by using large depth approximation .....	78
Figure 9	Rayleigh wave features for field due to point loading .....	79

# **CHAPTER 4**

## **PARALLEL IMPLEMENTATION OF A BOUNDARY ELEMENT ANALYSIS CODE FOR HALFSPACE ELASTODYNAMICS PROBLEMS**

### *Introduction*

An effective way to cope with the computationally-intensive issue of halfspace elastodynamic problems is to take advantage of computer technology. Among the many efficient special advances in computing is the one called parallel computing.

Since the early 1970s, computers consisting a number of separate processors, called parallel processors, began to appear. It has been apparent that parallel computing can provide an effective and efficient way to solve large-scale structural analysis problems and other problems which take long time to be solved via serial methodology [1].

Specifically for the Boundary Element Method (BEM), there are a number of papers on the parallel computing [2,3,4,10]. All researchers agree that BEM is very suitable for parallel programming because of the scalability of the method, i.e. the structure of BEM make it easy to divide the whole task into several parallel small independent tasks. For halfspace elastodynamics problems via the BEM, it is known that the amount of CPU time for forming the coefficient matrix is the major problem when Lamb's halfspace Green's function is used to formulate the BIE. This is due to the fact that Lamb's solution is available in an analytical form [5,6] which requires (numerical)

evaluation of infinite integrals with respect to frequency, the CPU time spent on just forming a boundary integral equation is increased significantly and often prohibitively. The purpose of this research is to provide a parallel scheme for BEM analysis for the halfspace problem, and to explore the great advantages of parallel computing with BEM.

The parallel computing for the present work was carried out on the IBM SP-2 in the national supercomputing center at Cornell University using PVM. PVM stands for parallel virtual machine which is a software system that permits a heterogeneous collection of UNIX workstations networked together to act as a single parallel computer [7]. Communication between processors takes place by message-passing in which data or other information are transferred between processors. The main advantage of PVM is its affordability and the substantial computing power of individual workstations.

The major work here is to design a parallel algorithm for BEM for the halfspace problem, and to reorganize and rewrite the code in the PVM environment to obtain a maximum performance gain.

There are two major steps in the BEM process for any problem:

1. Forming the coefficient matrix; this involves collocating at each nodal point, then numerically integrating over each boundary element. The coefficient matrix defines a governing linear system of equations for boundary value problem at hand.
2. Solving the linear system of equations.

The CPU time spent on each step is determined by the size of the problem and the kernels used in the BIE. Usually the size of the system equation increases nonlinearly with the size of the problem, so does the CPU time spent on solving the linear system of

equations. For large scale problems, step 2 will dominate. Thus parallization procedures for solving the linear algebraic system is essential. Fortunately, there is a large amount of work in the area of parallel-solving for linear algebra equations. Efficient algorithms such as parallel LU decomposition as well as standard routines can be obtained [8,9].

When the halfspace Green's function is used in the BIE formulation of a halfspace problem, the CPU time spent on step 1 dominates even for a very small-size problem based on few boundary elements. Thus the emphasis in this research is basically on the parallelization of step 1. Specifically, in this section, a parallel scheme is designed for the boundary element analysis code for elastodynamics problems using halfspace Green's function via PVM. The problem of radiation from a sphere in the halfspace is considered.

### ***BIE Formulations***

Consider a homogeneous, isotropic, elastic halfspace bounded by a flat halfspace surface  $S_H$  at  $z=0$ , which is traction free, as shown in Figure 1. The elastic material fills the halfspace  $z \geq 0$ . There is a finite obstacle  $B$  inside the halfspace with a surface  $S$ . In the region  $B'$ , exterior to  $B$  but within the halfspace, we assume that an elastic field exists in the form of a time harmonic displacement vector  $u_i(p, \mathbf{w})$ , which must satisfy the familiar Navier equation,

$$(c_1^2 - c_2^2)u_{j,ji} + c_2^2 u_{i,jj} + \mathbf{w}^2 u_i = 0 \quad (1)$$

where  $c_1$  and  $c_2$  are dilatational- and shear-wave speeds, respectively,  $\mathbf{w}$  is the circular frequency, and body forces are assumed to be zero. This field is assumed to arise from a prescription of boundary data on  $S$ .

The BIE for elastodynamic problems using halfspace Green's functions can be written as

$$C_{ij}(p)u_j(p) = \int_S [T_{ij}^H(p,q)u_j(q) - U_{ij}^H(p,q)t_j(q)]ds(q) + u_i^{inc} \quad (2)$$

where  $T_{ij}^H(p,q), U_{ij}^H(p,q)$  are traction and displacement Green's functions for a halfspace problem, also called Lamb's solution;  $u_j(q), t_j(q)$  are the displacement and traction respectively at point  $q$ ;  $S$  is the boundary of the inhomogeneity in the halfspace, usually the surface of the finite obstacle. For radiation by a sphere in the halfspace,  $S$  is the surface of the sphere, and  $u_i^{inc} = 0$ . Here we restrict ourselves to a radiation problem. The parallel scheme is equally applicable to a scattering problem. In eqn. (2)  $C_{ij}(p)$  is the coefficient tensor of the free term (cf. [11]) and is a function of the location of  $p$ . When  $p$  is inside  $B'$ , eqn. (2) is a representation integral which gives the solution at  $p$  in terms of boundary values of  $u_j(q), t_j(q)$  on  $S$ , and  $C_{ij}(p) = \mathbf{d}_{ij}$ . When  $p$  is on the boundary  $S$ , eqn. (2) is a BIE in which half of the pair of variables  $u_j(q), t_j(q)$  are prescribed for a well posed problem. The BIE (2) can be solved for the other half of the boundary data.

Indeed, in the BIE process, the first step is to put  $p$  on the boundary; the BIE is then solved for the unknown boundary data. In the second step, the solution at any point inside the domain  $B'$  can be obtained from the representation integral.

If we discretize the boundary and collocate at nodal points, the discretized form of the BIE is obtained as

$$[A]\{u(q_N)\} = [B]\{t(q_N)\}. \quad (3)$$

For a well posed elastodynamics problem, either  $u_j$  or  $t_j$  at any nodal point is given, so by rearranging the above equation, retaining the unknown variables on the left hand side of the equations, while moving all the known terms to the right hand side, we have the following linear algebraic equations:

$$[A] \{unknowns(q_N)\} = \{RHS\}. \quad (4)$$

After solving the above simultaneous equations for the unknowns at nodal points, all of the boundary values for  $u_j$  and  $t_j$  at all nodal points are obtained. Then we can calculate displacement or stresses at any field point by the boundary integral representation eqn. (2) with  $C_{ij}(p) = d_{ij}$ .

### ***Serial Execution***

The flowchart of the serial BEM code is as shown in Figure 2. The serial code includes 58 subroutines, and consists of 9970 lines of statement.

The test example is the problem of radiation from a sphere in the halfspace. The surface of the sphere is discretized into 8 triangular elements as shown in Figure 3.

A crude mesh was used for the sphere merely because this research was done as a class project. There exists a limitation about the problem size.

A profile study which can list the CPU times for each procedure indicates that most of the CPU time is spend in the functions called by subroutine cte3 in which the coefficient matrix is formed. To accurately record the CPU time, this serial code was executed on the Loadlevel where it is guaranteed that only one job is run at a time. It originally takes about 300 seconds to run the test problem. In order to concentrate on the

parallization, no serial optimization was done for the serial code. Instead, the intrinsic-O3 optimization flag was used when the code was compiled. This performs both the -O level optimizations and performs additional optimizations that are memory or compile-time intensive. The serial CPU time is then reduced to about 160 seconds (See Table 1).

### ***Parallel Implementation***

The boundary element analysis code is well suited for parallel execution for the following reasons:

1. The BEM code is coarse grained or has a large-scale granularity which means that large tasks can be performed independently in parallel. This is true especially for the code which use the halfspace Green's function, where forming the coefficient matrix costs most of the CPU time (>99.9% for the test example); and most of this part of the code can be run in parallel.

2. The BEM code also has a very good scalability in the part of it which consumes most of the CPU time. This means it is easy to separate the job into several jobs to be run on each processor parallely and independently. The task of forming the coefficient matrix is divided into several small tasks such that each small task calculates several columns of

Table 1 CPU time and performance for serial and parallel execution

	Wall clock time (seconds)	Speed up
Serial without -O3 option		
Run 1	302	
Run 2	296	
Run 3	296	
Run 4	296	
Run 5	302	
Serial with -O3 option		
Run 1	160	
Run 2	160	
Run 3	159	
Run 4	159	
Run 5	160	
Parallel execution with -O3 option		
Run 1	23	
Run 2	22	
Run 3	22	
Run 4	21	7.57
Run 5	23	

the coefficient matrix. For example, in the numerical example here, each processor forms the columns which correspond to the integration over one element.

3. The BEM code has parallel-data independence in the part of the code which consumes most of the CPU time. The data in the coefficient matrix are parallel independent too. Given the information of connectivity of a specific element and all the nodal points, each processor can calculate part of the coefficient matrix independently, and can send it back separately. This means each processor does not need to wait for data from other processors during the process.

Here are some considerations in parallel implementation:

1. The so-called Host/node configuration was used in this project, the host was responsible for the I/O process and passing necessary data to each node. Each node performed the integration over one boundary element for all nodal points. i.e. the node formed several columns of the coefficient matrix, and sent the results back to the host. Then the host performed the assembling of the coefficient matrix, solving of the system of equations and postprocessing of the results. Details are as indicated in the parallel code flowchart (see Figure 4).

2. Load balancing issues

By load balancing, we mean the assignment of tasks to the processors of the system is done in such a way that each processor is kept doing useful work as much as possible. The following are some considerations regarding load balancing.

a. Eight tasks were spawned at the beginning of the host program such that while the host program reads in model data, nodes can start to do some pre-calculations as to

calculate the shape functions and gaussian quadrature information etc. These pre-calculations are independent of the model data

b. The model data and boundary conditions are sent separately in two messages to allow some overlapping. i.e. while nodes were unpacking the data, host can read in some more data.

Based on the above considerations, the flowchart of the parallel code is as in Figure 4. As mentioned, the radiation problem from a sphere in the halfspace is considered. An eight-element mesh as shown in Figure 3 is used. In the parallel execution, eight workstations were used to solve this problem. A nearly perfect speedup (7.57) is obtained, The speedup is defined as the ratio of the execution time for a single processor and the execution time using multiple processors. Ideally, the speedup by using  $n$  processors could reach  $n$ , but the attainable speedup depends on the degree to which the serial program can be divided into independent (and parallel) tasks. The speedup also depends on the number and size of the messages passed and on the ratio of communication and computation time.

### *Conclusions*

By parallelizing the BEM code for halfspace elastodynamics problems, a very good speedup is obtained in this exercise. All of the work associated with this exercise indicates that boundary element analysis code is easy parallelize because of its coarse granularity, easy scalability and good data independence. Parallel computing can provide a way to solve halfspace scattering problems effectively and efficiently.

## *References*

1. A.K. Noor, Advances and trends in computational structure mechanics, Advances and Trends in Computational Mechanics (ASME, New York, 1986).
2. K.A. Kline, N.K. Tsao, and C.B. Friedlander, Parallel processing and the solution of boundary element equation, in Advanced Topics in Boundary Element Analysis (ASME, AMD Publication New York, 1985), 257-270.
3. A. Zucchi, S. Mukherjee, Vectorial and parallel processing in stress analysis with boundary element method, Int. J. Num. Meth. Engrg., 31 (1991) 307-317.
4. X.S. Zhang, T.Q. Ye, and R.P. Wang, Multidomain boundary element method and its parallelization, in M. Tanaka, Q. Du, and T. Honma, eds., Boundary Element Methods (Elsevier Science Publishers, Amsterdam, 1993).
5. R.A Roberts, Elastodynamic response of contacting fluid and solid half-spaces to a three-dimensional point load, Wave Motion, 12 (1990), 583-593.
6. L. Pan, F.J. Rizzo, Some efficient boundary integral strategies for wave problems in an elastodynamic halfspace, will submit to Comp. Meth. in App. Mech. and Eng.
7. J. Dongarra, W. Jiang, R. Manchek, V. Sunderam, PVM: Parallel Virtual Machine, A User's Guide and Tutorial for Networked Parallel Computing (The MIT Press, Cambridge, Massachusetts, 1994).
8. G. Golub, J.M. Ortega, Scientific Computing: an Introduction with Parallel Computing (Academic press Inc, San Diego, 1993).
9. IBM -Engineering and Scientific Library Guide and Reference, Release 3, IBM, Kingston, New York.

10. J.B Drake, and L.J. Gray, Parallel implementation of the boundary element method on the IPSC2 hypercube for electro-plating applications, Oak Ridge Laboratory, Technical Report ORNL-5615, Oak Ridge, Tennessee, 1988.
11. F. J. Rizzo, D. J. Shippy and M. Rezayat, A boundary integral equation method for time-harmonic radiation and scattering in an elastic half-space, ASME Winter Annual Meeting, Miami Beach, Florida, November, 1985.

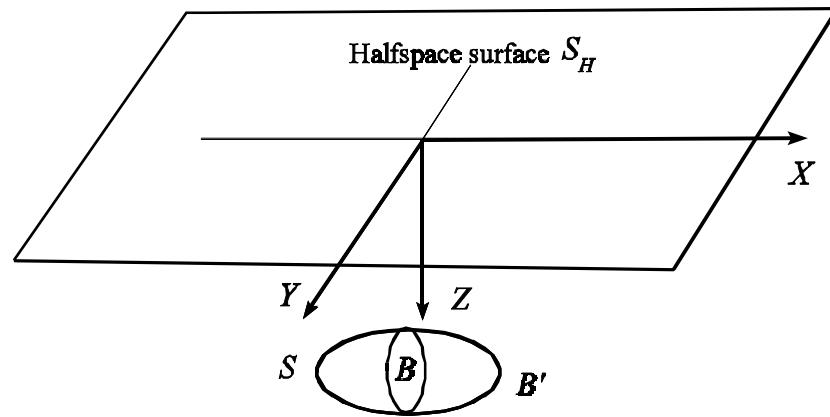


Figure 1 The halfspace problem

Figure 2 Serial code flow chart

Figure 3 Sphere discretization

Figure 4 Parallel code flow chart

Figure 3 Parallel code flow chart (continued)

**CHAPTER 4 PARALLEL IMPLEMENTATION OF A BOUNDARY  
ELEMENT ANALYSIS CODE FOR HALFSPACE ELASTODYNAMICS**

<b>PROBLEMS</b>	<b>80</b>
<b>Introduction</b>	<b>80</b>
<b>BIE Formulations</b>	<b>82</b>
<b>Serial Execution</b>	<b>84</b>
<b>Parallel Implementation</b>	<b>85</b>
<b>Conclusions</b>	<b>88</b>
<b>References</b>	<b>89</b>

## **CHAPTER 5**

# **ELASTODYNAMIC SCATTERING FROM A SURFACE-BREAKING CRACK**

### *Introduction*

Scattering of elastic waves by planar cracks is an important area of investigation in applied mechanics, especially in quantitative non-destructive evaluation (NDE). However, there are few solutions to three-dimensional scattering problems, and these are almost all for the special case of scattering by an internal penny-shaped crack [1]. A number of references using numerical methods, such as boundary elements, finite differences etc., can be found in [1].

The problem of scattering from a surface-breaking crack is of particular interest to NDE, and considerable effort has been devoted to obtaining numerical data for this problem. But most of the research has been done under two-dimensional (2D) assumptions, for example [2-4]. However, it was pointed out in [5] that if the crack dimensions are comparable to the width of the interrogating beam, the full three-dimensional problem must be considered.

The BEM is especially good for this class of problem because, as a numerical tool, it is valid under 2D or 3D assumptions, either semi-circular cracks or more general crack shapes, cracks which are inclined or perpendicular to the free surface, and in the low frequency, intermediate frequency or even high frequency range, if proper care is taken.

### ***Problem Description And the BIE Formulation***

The problem considered here is the scattering of a wave by a surface-breaking crack in the halfspace.

Consider a homogeneous, isotropic, elastic halfspace bounded by a flat halfspace surface  $S_H$  at  $z=0$ , which is traction free, as shown in Figure 1. Elastic material fills the halfspace  $z \geq 0$ . There is a semi-circular crack which is normal to and breaks the halfspace surface. We first consider the case in which the crack is insonified by a SV wavefield incident at an angle of  $\theta = 45^\circ$  (see Figure 2 for definition of  $\theta$ ). Because of the radiation condition, we solve this original problem in two steps as depicted in Figure 1. By convention, the crack surface is denoted by  $S_2$ , the truncated area on the halfspace surface is  $S_1$ .

In step 1, we assume there is no crack, and the halfspace is under the load of the incident wave. Both the displacement  $u_i^I$  and traction  $t_i^I$  on the fictitious crack surface can be obtained analytically [12]. Then in step 2,  $-t_i^I$  is applied on the crack surface, and the problem in step 2 becomes the problem for a halfspace with a surface-breaking crack under the load of crack-surface traction only. This problem can be solved by the boundary element method. It can be seen that the superposition of these two steps is equivalent to the original problem.

For crack problems or problems with a thin-body domain, the hypersingular boundary integral formulation (HBIE) is needed since the conventional BIE (CBIE) alone breaks down because of the degeneracy of the main coefficient matrix [7]. Incidentally, the HBIE is also used in dynamic analysis [6] to overcome the so called fictitious-frequency difficulties [8].

While the HBIE is very useful in solving problems with cracks or thin bodies, the process of

using HBIE presents more analytical and numerical difficulties than does the CBIE because the HBIE is one order higher in singularity for the kernel functions than those in the CBIE.

The HBIE can be obtained by taking spatial gradients of the CBIE and multiplying the resulting equation with the elastic modulus tensor  $E_{iklm}$  and the direction cosine of the normal vector at the source point  $n_{0k}$  [14]. The resulting HBIE for a radiation problem, involving tractions and displacements explicitly, has the form

$$t_i(p) = \int_S \left[ K_{ij}(p, q) t_j(q) - H_{ij}(p, q) u_j(q) \right] ds(q) \quad (1)$$

where the kernels are

$$K_{ij}(p, q) = E_{iklm} \frac{\mathcal{U}_{ij}(p, q)}{\mathcal{U}_{x_{0m}}} n_{0k}, \quad (2)$$

$$H_{ij}(p, q) = E_{iklm} \frac{\mathcal{T}_{ij}(p, q)}{\mathcal{U}_{x_{0m}}} n_{0k} \quad (3)$$

where  $U_{ij}(p, q)$  and  $T_{ij}(p, q)$  are kernels for the CBIE. Details about the derivation of HBIE and the expression for the kernels can be found in [14].

For the halfspace surface-breaking crack problem, the boundary consists of four portions, i.e.,  $S = S_1 \cup S_R \cup S_2^+ \cup S_2^-$  as in Figure 2.

The HBIE for the surface-breaking crack problem can be then expanded as

$$\begin{aligned} t_i(p) = & \int_{S_1} \left[ K_{ij}(p, q) t_j(q) - H_{ij}(p, q) u_j(q) \right] ds(q) \\ & + \int_{S_2^+} \left[ K_{ij}(p, q^+) t_j(q^+) - H_{ij}(p, q^+) u_j(q^+) \right] ds(q^+) \\ & + \int_{S_2^-} \left[ K_{ij}(p, q^-) t_j(q^-) - H_{ij}(p, q^-) u_j(q^-) \right] ds(q^-) \\ & + \int_{S_R} \left[ K_{ij}(p, q) t_j(q) - H_{ij}(p, q) u_j(q) \right] ds(q). \end{aligned} \quad (4)$$

Note

$$K_{ij}(P, Q^+) = K_{ij}(P, Q^-),$$

$$H_{ij}(P, Q^+) = -H_{ij}(P, Q^-).$$

If we define

$$\Delta u_j(q) \equiv u_j(q^+) - u_j(q^-),$$

as the displacement discontinuity across the two crack surfaces, and

$$\Sigma t_j(q) \equiv t_j(q^+) + t_j(q^-),$$

as the sum of tractions on the two crack surfaces. Also notice that as  $R \rightarrow \infty$ ,

$$\int_{S_R} \left[ K_{ij}(p, q) t_j(q) - H_{ij}(p, q) u_j(q) \right] ds(q) \rightarrow 0. \quad (5)$$

The HBIE for the surface-breaking crack problem can be written as

$$\begin{aligned} t_i(p) &= \int_{S_1} \left[ K_{ij}(p, q) t_j(q) - H_{ij}(p, q) u_j(q) \right] ds(q) \\ &+ \int_{S_2^+} \left[ K_{ij}(p, q) \Sigma t_j(q) - H_{ij}(p, q) \Delta u_j(q) \right] ds(q). \end{aligned} \quad (6)$$

For the present loading condition,  $t_j(q) = 0, \forall q \in S_1$ ,  $\Sigma t_j(q) = 0, \forall q \in S_2$ . By moving all

of the terms to one side of the equation, the HBIE used here in particular is

$$t_i(p) + \int_{S_1} H_{ij}(p, q) u_j(q) ds(q) + \int_{S_2^+} H_{ij}(p, q) \Delta u_j(q) ds(q) = 0. \quad (7)$$

If  $u_j(q)$ ,  $\Delta u_j(q)$  are taken as the variables on  $S_1$  (the halfspace surface) and  $S_2^+$  (the crack surface) respectively, the HBIE Eqn (7) can be written in a compact form:

$$t_i(p) + \int_S H_{ij}(p,q) f_j(q) ds(q) = 0 \quad (8)$$

where  $S = S_1 \cup S_2^+$ , and

$$\begin{aligned} f_j(q) &= u_j(q), \quad \forall q \in S_1, \\ f_j(q) &= \Delta u_j(q), \quad \forall q \in S_2^+. \end{aligned} \quad (9)$$

Eqns (8) and (9) indicate that for problems with a crack, if the HBIE is used, only one surface of the crack needs to be discretized and collocated. After solving this equation, what we obtain on the crack surface is the displacement discontinuity instead of the displacement itself.

The kernels in the HBIE are singular in  $r$  with orders

$$\begin{aligned} K_{ij}(P,Q) &= O\left(\frac{1}{r^2}\right), \\ H_{ij}(P,Q) &= O\left(\frac{1}{r^3}\right), \end{aligned}$$

that is, one order higher than those in the CBIE. The first and second integrals in Eqn (1) are thus interpreted (et. seq.) as Cauchy principal values [16] and Hadamard finite parts [17,18], respectively.

Regularization of the HBIE formula (8) is needed before discretization in order to use Gaussian quadrature to evaluate the integrals. However, because only one surface of the crack needs to be modeled, the integral identities used for global regularization for problems having a closed surface boundary no longer hold [15]. The global regularization can not be used anymore; instead the local regularization using line integrals is needed. The detailed process of local regularization can be found in [9].

To get the local-regularized form of HBIE eqn. (8), first write it as

$$t_i(p) + \int_{S-\Delta S} H_{ij}(p,q) f_j(q) ds(q) + \int_{\Delta S} H_{ij}(p,q) f_j(q) ds(q) = 0 \quad (10)$$

where  $S$  is the boundary formed by singular elements which have the collocation point  $p$  as one of the nodal points;  $S-\Delta S$  is the rest of the boundary. The first integral in eqn (10) is regular, the second integral can be regularized locally as:

$$\begin{aligned} \int_{\Delta S} H_{ij}(p, q) f_j(q) ds(q) &= \int_{\Delta S} [H_{ij}(p, q) - \bar{H}_{ij}(p, q)] f_j(q) ds(q) \\ &+ \int_{\Delta S} \bar{H}_{ij}(p, q) \left[ f_j(q) - f_j(p) - \frac{\partial f_j}{\partial x_a}(p) (\mathbf{x}_a - \mathbf{x}_a^p) \right] ds(q) \\ &+ f_j(p) \int_{\Delta S} \bar{H}_{ij}(p, q) ds(q) \\ &+ \frac{\partial f_j}{\partial x_a}(p) \int_{\Delta S} \bar{H}_{ij}(p, q) (\mathbf{x}_a - \mathbf{x}_a^p) ds(q). \end{aligned} \quad (11)$$

where  $\bar{H}_{ij}(p, q)$  is the static kernel, and the last two integrals are computed using a line integral [9].

Notice for the present problem that,

$$\begin{aligned} t_i(p) &= 0, \quad \forall p \in S_1, \\ t_i(p) &= -t_i^I(p), \quad \forall p \in S_2^+. \end{aligned}$$

The discretized form of equation (10) can be written in matrix form as

$$\begin{bmatrix} A_{11} & A_{12} \\ A_{21} & A_{22} \end{bmatrix} \begin{Bmatrix} u_1 \\ \mathbf{D}u_2 \end{Bmatrix} = \begin{Bmatrix} 0 \\ t_2^I \end{Bmatrix} \quad (12)$$

Where:

$A_{11}$  is the coefficient matrix when collocating on  $S_1$  and integrating on  $S_1$ ,

$A_{22}$  is the coefficient matrix when collocating on  $S_2$  and integrating on  $S_2$ ,

$A_{12}, A_{21}$  are cross terms when collocating and integrating on different surfaces.

$u_1$  is the displacement vector on the halfspace surface, and  $Du_2$  is the crack opening displacement vector on the crack surface.

The solution of equation (12) yields the crack opening displacement vector over the  $S_2$  elements and the displacement vector on the flat surface of the halfspace.

After the crack-opening displacement is obtained, the scattered fields in the farfield or any points inside the halfspace can be computed by using the boundary integral representation, i.e.

$$u_j^s(P) = \int_{S_2} T_{ij}^H(P, q) \Delta u_j(q) ds(q). \quad (13)$$

in which  $T_{ij}^H$  is the halfspace Green's function as in [20]. Thus the integration is taken only over the finite surface  $S_2$  since the presence of the traction-free halfspace surface is accounted for in the halfspace Green's function. That is,  $T_{ij}^H(p, q) = 0$ , whenever  $q$  is on  $S_H$  ( cf. [21] ). The scattering amplitudes can then be calculated from the scattered displacement field [23].

Also, Auld's electromechanical reciprocity relationship [22, 23] can be used to predict the flaw induced signal change  $d\Gamma_F$  in the received signal due to the presence of a flaw.  $d\Gamma_F$  is found to be a function of particle velocity  $\dot{u}$  and stress tensor  $\dot{\mathbf{t}}$  for state "a" --transmitting transducer illuminating the medium with the flaw present, and for state "b" --receiving transducer acting as a transmitter with the flaw absent. Specifically,

$$d\Gamma_F = \frac{1}{4P} \int_S [\dot{u}_a \cdot \dot{\mathbf{t}}_b - \dot{u}_b \cdot \dot{\mathbf{t}}_a] \cdot \vec{n} ds \quad (14)$$

where  $P$  is the incident electrical power.  $S$  is any closed surface which contains the flaw and

can be the flaw surface itself in the BEM calculation [23];.  $\bar{n}$  is the normal direction of the surface  $S$ . In the frequency domain

$$d\Gamma_F(\mathbf{w}) = \frac{i\mathbf{w}}{4P} \int_S [u_a \cdot \bar{\mathbf{t}}_b - u_b \cdot \bar{\mathbf{t}}_a] \cdot \bar{\mathbf{n}} ds . \quad (15)$$

In this paper, we present the normalized Auld voltages, as

$$d\Gamma_F(\mathbf{w}) = \int_S [u_a \cdot \bar{\mathbf{t}}_b - u_b \cdot \bar{\mathbf{t}}_a] \cdot \bar{\mathbf{n}} ds . \quad (16)$$

To better model the crack tip behavior, we use the square-root built in eight-node quadrilateral (nonconforming) elements along the crack tip [24].

$$\begin{aligned} N = & c_1 \sqrt{(1+\mathbf{h})} + c_2 \mathbf{x} \sqrt{(1+\mathbf{h})} + c_3 (1+\mathbf{h}) + c_4 \mathbf{x}(1+\mathbf{h}) \\ & + c_5 \mathbf{x}^2 \sqrt{(1+\mathbf{h})} + c_6 (1+\mathbf{h})^2 + c_7 \mathbf{x}^2 (1+\mathbf{h}) + c_8 \mathbf{x}(1+\mathbf{h}) \end{aligned} \quad (17)$$

The basis functions in equation (17) are selected such that  $N$  goes to zero at the crack tip.

### ***Discretization Considerations And Numerical Results***

Numerical experiments with discretizations of  $S_I$  over circular regions with radii 2a, 3a, 5a, 7a, 8a and also over the elliptical region 2.5a x 3a, as a truncated model of  $S_H$  have been done (See Figure 3). Table 1 shows the maximum amplitudes of the crack opening displacement (COD) and the amplitude of the AULD voltage for three different discretizations for  $K_I a = 1$ . The solid is taken to be Aluminum ( $C_L = 6320 \text{ m/s}$ ,  $C_S = 3080 \text{ m/s}$ ). It is observed that for low to intermediate frequency scattering from a crack, a discretization which models 2.5ax3a of the free surface, as in Figure 3, gives convergent results. The discretization in Figure 3 has 68 elements on the flat surface and 26 elements on the crack surface. The

characteristic mesh size is chosen such that no element spans a distance greater than  $1/6$  of the wave length of the incident wave. Smaller elements along the crack tip on the crack surface as well as in the vicinity of the crack edge on the halfspace surface were used in order to capture the singularity along the crack tip.

Nonconforming elements as in Figure 4 were used because of perceived smoothness requirements needed with HBIEs [8]. The size of the coefficient matrix of the problem increases rapidly with the number of nonconforming elements since the total number of nodes for a discretization of  $M$  nonconforming elements is exactly  $8*M$ , if only 8-node quadrilateral elements are used, while for a discretization using conforming elements, the number of nodes is approximately  $3*M$ . Thus the ability to increase  $M$  in the nonconforming case is restricted, before memory and CPU demands become excessive. How to justify use of conforming elements with the HBIE such that we can use more elements for the same size of the problem is therefore a future research area of considerable interest [19].

Figure 5 shows COD variations on the crack surface. The semi-circle in Figure 5 represents the semi-circular cross section of the crack. Both the COD variation along the mouth of the crack and the depth of the crack are plotted in Figure 5. Since non-conforming elements are used, the results at nodal points are extrapolated to the corner point to make the plot. The discontinuity in two adjacent elements is thus an artifact of the non-conforming elements.

Table 1 Maximum CODs for some discretizations

Mesh Description	Modeled area on the halfspace surface	Elements		Maximum COD at nodal points	Result from AULD integration
		on the halfspace surface	on the crack surface		
48 element mesh	5ax5a	36	12	0.5718	0.0290
68 element mesh	7ax7a	48	20	0.5912	0.0299
94 element mesh	3ax2.5a	68	26	0.5877	0.0296

It can be seen that the largest amplitude of the COD occurs along the depth of the crack and in-between the crack edge and the crack mouth. This is reasonable considering the loading and the boundary conditions at the crack edge and crack mouth.

Figure 8 and Figure 9 show the magnitudes of the P-wave and S-wave farfield scattering amplitude respectively. These are obtained through the following process: first the farfield scattered displacement is calculated using the crack opening displacements on the crack surface in eqn. (13); then the scattered displacement is decomposed into P-wave and S-wave components; finally the farfield P-wave and S-wave scattering amplitudes are obtained according to the definition of scattering amplitude (See [1] or [23]). In Figure 8 and Figure 9, the variation of the magnitudes of these scattering amplitudes, for the observation angle  $0 < \Psi \leq 90$  (See Figure 2 for the definition of  $\Psi$ ), is plotted. The plots in Figure 8 and Figure 9 can be extended to  $90^\circ \leq \Psi < 180$  because of the symmetry about the  $z$ -axis.  $\Psi = 0^\circ$  and  $\Psi = 180^\circ$  corresponding to the observation points on the halfspace surface. The data at those two points are not available because when calculating the field for such points on the halfspace surface, chances are that some integration points are very close to the halfspace surface too. In the halfspace Green's function code we used for the present research, such a combination of P (interior point) and q (Gaussian quadrature point on the elements on the crack surface) will cause numerical instability. Three curves in each figure come from the three different discretizations, and thus different sizes of truncation for the halfspace surface. It can be seen that the results from these three different discretizations converge very well.

The BEM was employed to investigate the halfspace surface-breaking crack problem in [5] also, and constant elements were used. Obviously this is a very crude approximation

because of the discontinuities inherent in assuming both the displacement and traction constant over elements. The convergence of the numerical solution in [5] was based on the convergence in the farfield only. We report convergence in the COD data as well as the farfield.

Also, here we use locally-quadratic boundary elements. Moreover, unlike [5], we prepare our hypersingular integrals for numerical integration before rather than after discretization of the crack into elements. This is more straightforward analytically and, no doubt, this contributes to improved accuracy as well.

### ***Partitioning Method and Library Idea***

Because of the presence of the crack, we need a fine mesh to get good results, but a fine mesh easily used up the memory of the computer because of the mentioned properties of nonconforming elements. To deal with this issue, note first that, as with the halfspace scattering problem in [20], the existence of two separate boundaries gives us the explicit matrix equation as in eqn. (12). Thus, again, the idea of partitioning can be applied here. A slightly different way of doing partitioning is implemented here, than in Chapter 3, specifically for the halfspace surface-breaking crack problem, in order to increase the capability to solve a larger problem on the same computer. Another algorithm is used to solve the problem in step 2 via three sub-steps. In the first sub-step, we collocate only on the flat surface, form  $A_{11}$  and  $A_{12}$ , and then find  $A_{11}^{-1}$  (LU decomposition of  $A_{11}$ ) and finally store all of these matrices. In the second sub-step we collocate only on the crack surface, form  $A_{21}$  and  $A_{22}$ , and store

them too. In the final sub-step, we read in all of the sub-matrices and solve a reduced system of equations to get the crack opening displacement  $\mathbf{Du}_2$ . Specifically:

Sub-step 1:

Collocating on the flat surface, notice that

$$t_i(p) = 0, \quad \forall p \in S_1. \quad (18)$$

We get

$$[A_{11}]\{u_1\} + [A_{12}]\{\Delta u_2\} = \{0\}, \quad (19)$$

$$\{u_1\} = -[A_{11}]^{-1}[A_{12}]\{\Delta u_2\}. \quad (20)$$

Sub-step 2:

Collocating on the crack surface, notice that

$$t_i(p) = -t_i'(p), \quad \forall p \in S_2 \quad (21)$$

Then we have the discretized form of equation as:

$$[A_{21}]\{u_1\} + [A_{22}]\{\Delta u_2\} = \{t_2'\}. \quad (22)$$

In this step, we form matrices  $[A_{21}]$  and  $[A_{22}]$  only, and store them.

Sub-step 3:

when eqn.(20) is plugged into eqn. (22), we have

$$[A_{22}]\{\mathbf{Du}_2\} - [A_{21}][A_{11}]^{-1}[A_{12}]\{\mathbf{Du}_2\} = \{t_2'\} \quad (23)$$

$$\left([A_{22}] - [A_{21}][A_{11}]^{-1}[A_{12}]\right)\{\Delta u_2\} = \{t_2'\}. \quad (24)$$

In sub-step 3, all the sub-matrices are read in, a new coefficient matrix and new known vector are calculated according to eqn. (24), and the crack opening displacements  $\Delta u_2$  is calculated.

By doing the whole problem in three sub-steps, the memory requirement is reduced because only two sub matrixes of the whole BIE coefficient matrix are formed in each sub-step. The memory needed is then approximately half of the requirement of the old scheme, for a given discretization. That means we gain the capability to deal with a mesh which is almost twice as fine as the finest mesh in the old scheme.

The result of a mesh with 126 elements in total, which is beyond the capacity of the computer by using old scheme, is presented in Figure 6. This mesh has the same pattern of discretization on the top surface as in Figure 3 and a finer discretization on the crack surface (See Figure 5).

### *Discussion*

The problem of scattering from a halfspace surface-breaking crack is solved here using the boundary element method. The fullspace fundamental solution is used in the formulation of the BIE. Therefore the halfspace surface is also one of the boundary surfaces for this problem, and consequently discretization and truncation on the halfspace surface are needed. As in [20], it is observed that the boundary solutions converges very quickly. However, the field solution depends on the size of the truncation, if the *fullspace* fundamental solution is also used in the representation integral. This is consistent with the conclusions reported in [20]. Thus, for the solutions at field points, an integral representation using the *halfspace* Green's function is needed, and convergence is also observed.

The Green's function library idea may be applied to this class of problems as follows: make an accurate discretization of the halfspace surface, obtain  $A_{11}^{-1}$ , and store this large matrix so that it can be reused over and over again with different sizes and shapes of cracks. As before,  $A_{11}^{-1}$  is the main ingredient in a so-called discretized Green's function for the crack problem. This idea is becoming attractive as storage and retrieval of mass-amounts of data become easier and cheaper.

Additional research for this category of halfspace surface-breaking crack problems is clearly facilitated by the methods of this chapter. As stated before, the BEM as a numerical tool, is valid for either 2D or 3D, semi-circular cracks or for more general shapes, and cracks which are inclined or perpendicular to the free surface.

### *References*

1. L.W. Schmerr, Ultrasonic NDE--A Modeling Approach, Preprint, 1993.
2. J. Dominguez, Boundary Elements in Dynamics (Elsevier Applied Science, Amsterdam, 1994)
3. D.A. Mendelsohn, J.D. Achenbach, L.M. Keer, Scattering of elastic waves by a surface-breaking crack, *Wave Motion*, 2 (1980) 277-292.
4. S.K. Datta, A.H. Shah, Ultrasonic scattering by planar and non-planar cracks, in , D.O. Thompson. and D.E. Chimenti, eds., *Review of Progress in Quantitative Nondestructive Evaluation*, 6A (Plenum Press, New York, 1986) 69-78.

5. D.E. Budreck, Three-dimensional elastodynamic scattering from internal and surface-breaking cracks by boundary integral equation methods, PhD Dissertation, Northwestern University, 1988.
6. D.E. Beskos, Boundary Element methods in Dynamic Analysis, *Appl. Mech. Rev.*, 40(1), 1-23.
7. G. Krishnasamy, F.J. Rizzo and Y. Liu, Scattering of acoustic and elastic waves by cracklike objects: the role of hypersingular integrals, in D. O. Thompson and D. E. Chimenti, eds., *Review of Progress in Quantitative Nondestructive Evaluation*, 11A (Plenum Press, 1991).
8. G. Krishnasamy, L.W. Schmerr, T.J. Rudolph and F.J. Rizzo, Hypersingular boundary integral equations: some applications in acoustic and elastic wave scattering, *J. App. Mech.*, 57(1990) 404-414.
9. Y. Liu, D. Zhang and F.J. Rizzo, Nearly singular and hypersingular integrals in the boundary element method, in C.A. Brebbia and J.J. Rencis, eds., *Boundary Elements XV, Proc. of the 15th Int. Conf. on Boundary Elements*, (Computational Mechanics Publications, Worcester, MA, 1993), 453-468.
10. D.E. Budreck, R.A. Roberts, Elastodynamic scattering from a three-dimensional crack in a fluid-loaded halfspace, in D.O. Thompson and D.E. Chimenti, eds., *Review of Progress in Quantitative Nondestructive Evaluation*, 11 (Plenum Press, New York, 1992).
11. R.A. Roberts, Elastodynamic scattering by a surface-breaking void, *J. Acoust. Soc. Am.* 85(2), (1989), 561-566.

12. J.D. Achenbach, Wave Propagation in Elastic Solids, (North-Holland Pub, Amsterdam. Co., 1973).
13. D.S. Jones, Boundary integrals in elastodynamics, IMAJ. Appl. Math., 34(1985), 83-97.
14. Y.J. Liu, Development and applications of hypersingular boundary integral equations for 3-D acoustics and elastodynamics, Ph.D. Dissertation, University of Illinois at Urbana-Champaign, 1992.
15. Y.J. Liu, and T.J Rudolphi, Some identities for fundamental solutions and their applications to non-singular boundary element formulations, Engineering Analysis with Boundary Element, 8(6), (1991).
16. N.I. Muskhelishvili, Singular Inetgral Equations (P. Noordhoff N. V., Groningen, Holland, 1953).
17. J. Hadamard, Lectures on Cauchy's Problem in Linear Partial Differential Equations (Dover, New York, 1952)
18. G. Krishnasamy, The boundary element method applied to static and dynamic crack problems using hypersingular boundary integral equations, PhD Dissertation, Iowa State University, 1990.
19. P.A. Martin, F.J. Rizzo, Smoothness-relaxation strategies for singular and hypersingular integral equations, Preprint.
20. L. Pan, F.J. Rizzo and P.A. Martin, Some efficient boundary integral strategies for wave problems in an elastodynamic halfspace, will submit to Computer Methods in Applied Mechanics and Engineering.

21. K. Aki and P.G. Richards, Quantitative Seismology, Vols. 1,2 (W.H. Freeman, San Francisco, 1980).
22. B.A. Auld, General electromechanical reciprocity relations applied to the calculation of elastic wave scattering coefficients, *Wave Motion*, 1 (1979), 3-10.
23. P.J. Schafbuch, Application of the boundary element method to elastic wave scattering problems in ultrasonic nondestructive evaluation, PhD Dissertation, Iowa State University, 1991.
24. Z.H. Jia, D.J. Shippy and F.J. Rizzo, Three-dimensional crack analysis using singular boundary elements, *Int. J. Numer. Methods Eng.*, 28 (1989), 2257-2273.

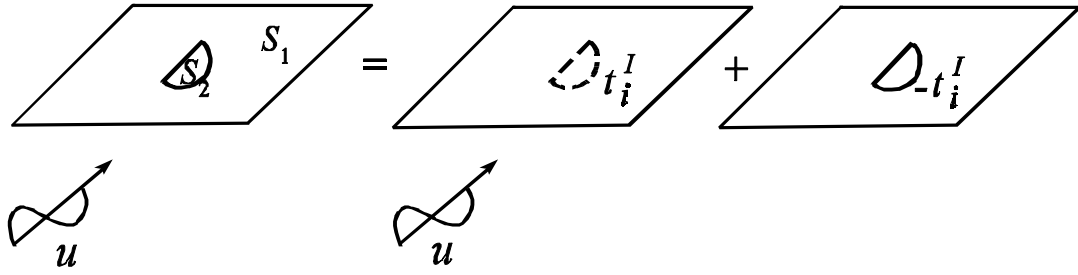


Figure 1 Halfspace surface breaking crack problem

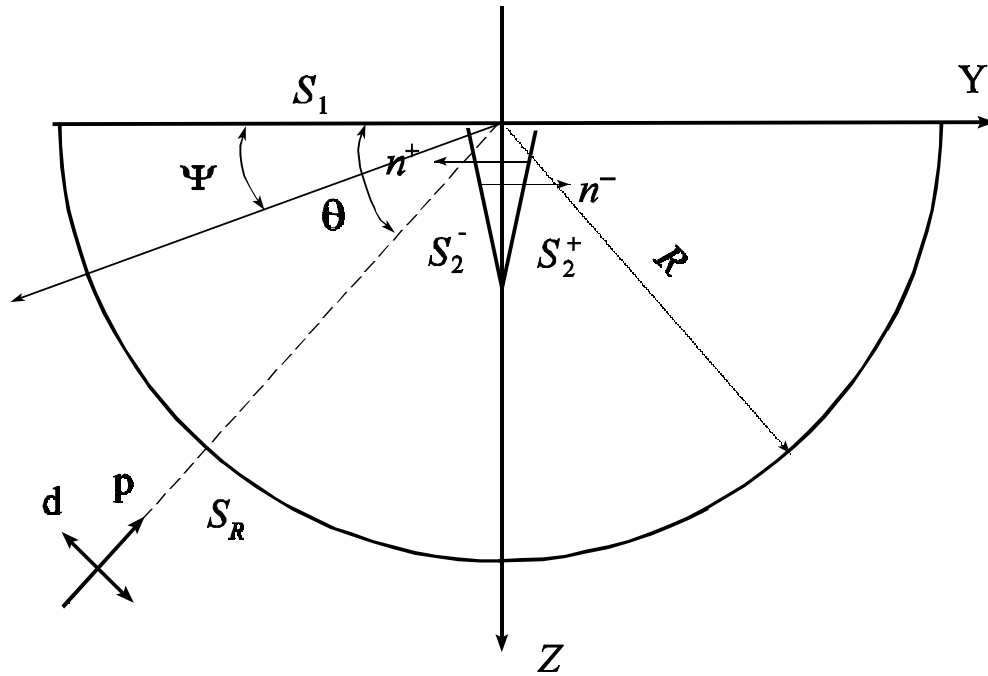


Figure 2 Halfspace surface-breaking crack

Figure 3 A typical mesh (94 elements in total)

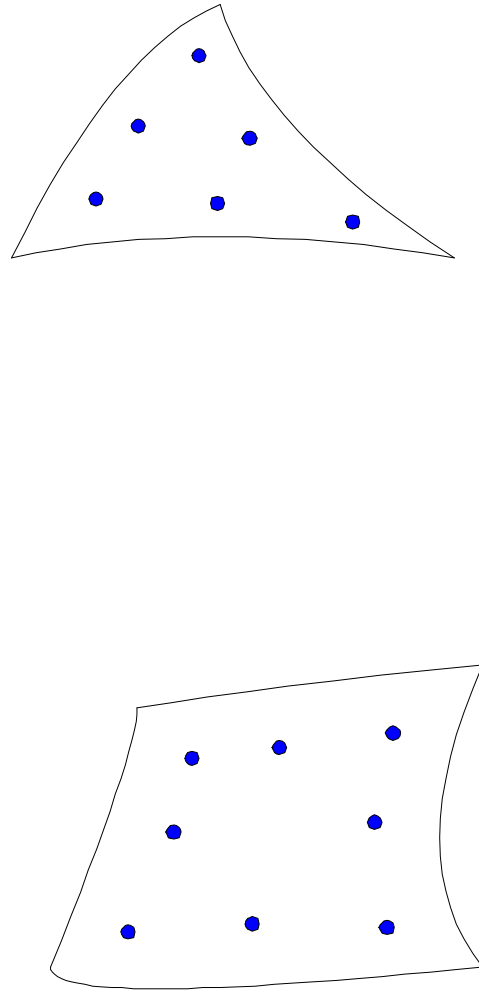


Figure 4 Triangular and quadrilateral nonconforming elements

Figure 5 CODs from 3 different discretizations

Figure 6 COD from 126 element mesh

Figure 7 126 element mesh

Figure 8 Farfield P-wave scattering amplitude

Figure 9 Farfield S-wave scattering amplitude

CHAPTER 5 ELASTODYNAMIC SCATTERING FROM A SURFACE-BREAKING CRACK .....	96
Introduction.....	96
Problem Description And the BIE Formulation ....	97
Discretization Considerations And Numerical Results.....	103
Partitioning Method and Library Idea.....	107
Discussion .....	109
References .....	110

## SUMMARY AND CONCLUSIONS

In this work, we show the explicit relation between the BIE/BEM method of solution and construction of the exact or region-dependent Green's function, for problems governed by linear elliptic partial differential equations. The exact Green's function for the problem and the unknown boundary variables on the boundary satisfy the same BIE but with a different known vector. As a consequence, the representation integral for the BIE solution of the BVP may be written in a form which contains a precise expression for the exact Green's function. This provides a way to construct a numerical approximation to an exact Green's function (a discretized Green's function) for problems for which an analytical Green's function is not available. Indeed, it is shown that in using the BIE method to solve a given BVP, one has in fact constructed the discretized Green's function for the domain. A number of ingredients in the BEM in combination may now be interpreted as a numerical approximation to the exact Green's function.

When using BEM to obtain the discretized Green's function, there is no restriction on the configuration (2D or 3D), no restriction on boundary condition and no restriction on the physical nature of the problem as long as it is a problem governed by linear elliptic partial differential equations. Thus the BEM, a well developed numerical tool regarded as useful in a particular way, can now be regarded explicitly as a vehicle to construct the discretized Green's function for any relevant problem.

Specifically, it is made clear that for a one-surface BVP, the inverse of the coefficient matrix ( $A^{-1}$ ) is the key ingredient in the discretized Green's function for the BVP. For

problems with two surfaces as the boundary, a sub-matrix of the coefficient matrix can be interpreted as the main ingredient of the partial Green's function for the problem as well. Finding the solution of a BVP using a partial Green's function is facilitated by the partitioning process described in Chapter 3. Indeed, suppose that one of the surfaces is larger and more complex than the other. One can construct the inverse of the sub-matrix associated with the large surface, and this is usually the key and most computationally-intensive ingredient in the BEM solution of a BVP with two surfaces. This requires a mesh, a code and expertise to get a reliable sub-matrix inverse (really an LU decomposition). The rest of the solution process usually involves a simple mesh on a small simple surface, at most, plus matrix multiplications based on formulas for numerical quadrature. This strategy is equivalent to creating a library of numerical approximations to exact partial-Green's functions for repeated use. Modern technology for storage of massive amounts of data, on CDs or on central storage, accessible via networks, would suggest that at least some heavy computing of this type can be 'done in advance', the results of which could be made available to non expert users.

The library idea for halfspace problems using the freespace fundamental solution involves forming an accurate discretization on the halfspace surface, obtaining the part of the coefficient matrix associated with the truncated halfspace surface model, and storing the inverse (LU decomposition) of that coefficient matrix for repeated use.

Two classes of problems are considered here as the application of BEM and discretized Green's function library. One is the application of the BEM to the analysis of 2D micromechanical behavior of fiber-reinforced composites. A BEM model for predicting 2D micromechanical behavior of fiber-reinforced composites is developed based on models for

both perfectly-bonded and imperfectly-bonded materials in a unit cell. The idea of a library of Green's functions and the entries for the library for fiber-reinforced composites is discussed.

The other class of problems considered here is the halfspace problem. BIE formulations using both the Stokes fundamental solution and the Lamb fundamental solution are used and compared. Strategies, based on the BEM for halfspace elastodynamics problems, are suggested and demonstrated to take advantage of the best features of the fullspace Stokes solution and halfspace Lamb's solution. The partitioning method is employed to explore the practicality of the library idea for halfspace problems..

Also, the scattering from a halfspace surface-breaking crack is considered in this thesis. Although this problem also belongs to the halfspace problem category, the necessity to use hypersingular integral equations for the crack problem brings more complexity both theoretically and numerically. Nevertheless, the conclusions about effective strategies for both problems are quite consistent. Specifically, when the fullspace fundamental solution is used in the BIE formulation, the truncation on the halfspace surface has a small effect on the boundary solution and quite a big effect on the solution at field points. So in order to get a reliable solution at field points, the halfspace Green's function rather than the fullspace one is advised to be used in the representation integral. The conclusions about using the fullspace Green's function and halfspace Green's function allows us to find boundary solutions using fullspace fundamental solution with confidence, and then use the halfspace Green's function to find field quantities.

After accurate boundary values are obtained, it is possible to use some asymptotic expressions to approximate field quantities. In the halfspace problem, how to use the

Rayleigh wave representation and boundary solutions from the BIE to approximate the farfield are indicated. How to use the boundary data from the BEM to construct an appropriate Rayleigh wave representation is an interesting topic by itself. These are all topics for future research.

Another interesting problem is the halfspace inclusion problem. Imagine instead of a void inside the halfspace, there exists an inhomogeneity of another material inside the halfspace. This is also an important problem from non-destructive evaluation point of view.

For the halfspace surface-breaking crack problem, the HBIE formulation allows us to solve for the scattered fields from cracks of any shape. Future work in the area of inclined, or curved, or multiple crack problems, with comparison with experimental data would be useful and is in the planning stages.

Finally, it is interesting to the author to note that the classical mathematical ideas for BVPs, leading to Green's function representations, integral formulas, and boundary integral equations, etc. took on a new significance in about 1965 with the fairly-wide availability of the digital computer. 'Old mathematics' developed for a different (largely analytical) purpose took on a 'new dress' and a new practical significance. The BEM has embodied that significance for years. Similarly, now in the middle 1990s, the BEM, with all of its customary need for expertise and heavy computing demands takes on a new significance with the wide availability of large amounts of storage and rapid data transfer. One can now, with some advance planning, have a considerable amount of heavy computing done in advance, by experts, with the results put in a library of discretized Green's functions. The fruits of this activity by experts is thus made available to non experts, for easy analysis and design of a variety of

physical systems. Thus, 'computer modeling' via the library idea follows a long-time well-understood trend in technological development, namely, 'a sophisticated tool is made available for easy use, to users who need not have the knowledge, skills, resources, nor the inclination to make the tool themselves.' Developing a user-friendly interface for different categories of problems is certainly an important development and this is ongoing at Iowa State right now.

**APPENDIX A**

**ELASTIC WAVE ANALYSIS SPHEROID (EWAS) LIBRARY**

**USER'S MANUAL**

Contents

PART I GENERAL INFORMATION ABOUT EWAS LIBRARY

PART II SOFTWARE INSTALLATION

PART III USING THE LIBRARY

PART IV EXAMPLE / DEMONSTRATION

***PART I GENERAL INFORMATION ABOUT EWAS LIBRARY***

Elastic Wave Analysis Spheroid Library (EWAS LIBRARY) is a library of coefficient Matrices which govern the scattered elastic field from spheroidal voids( see figure 1(a) and 1(b)). Matrices for spheroids with geometries shown in Table 1, incident wave numbers which range from 0.5 to 5, are available for this preliminary version of EWAS library. With the associated library software, a user of this library can compute the elastic field from spheroidal voids by simply typing the following information.

Type of wave

\* Incident angle

\* Wave number

\* Geometry of the spheroid

Results include:

- \*Boundary quantities (total displacement) at boundary element nodes

- \*The result from the AULD integral

- \*Scattered displacement for particular exterior points

- \*Farfield scattering P-wave and S-wave amplitude plots

At present, the library software has the capability to deal with plane waves (P-waves and S-waves) and Gauss-Hermit waves, and it is designed in such a way that if a user wants to investigate some other kind of wave, the only thing necessary is to replace the subroutine "pfield" with a new subroutine for calculating the displacement field and traction field at the nodes.

Having done numerical experimentation and comparison, we choose a 96 element, 194 node boundary element discretization (see Figure 2(a) and 2(b)) for a nondimensional shear wave number  $k_1 a$  less than 6. A 192 element, 386 node boundary element discretization (see Figure 3(a) and 3(b)) should be used when matrices are constructed for  $k_1 a$  greater than or equal to 6. This will be done in the future. This preliminary version of the EWAS library is limited to the scattering of a plane wave from a spheroid in elastic media with poisson's ratio.

## ***PART II SOFTWARE INSTALLATION***

The EWAS library includes a set of matrix data and the associated library software. Matrix data should be put in directory `~/lib/spheroid/Matrix`. Each matrix is of the size 2716924 bytes. All the matrices are named as `elexyz096nn.mat` where `xyz` are geometric

Table 1 Present shape and wavenumber

eccentricity	$k_1 a=1$	$k_1 a=2$	$k_1 a=3$	$k_1 a=4$	$k_1 a=5$
1:1:1	Yes	Yes	Yes	Yes	Yes
3:3:1	Yes		Yes		Yes
5:5:1	Yes	Yes	Yes	Yes	Yes

parameters for x,y,z direction respectively, nn is the wavenumber. For example, ele33109601.mat is the matrix data file for a 3:3:1 spheroid, and the incident wavenumber  $k_1 a$  is 1. The software includes a makefile called "Makefile" which performs the compiling and linking for all codes, a batch file called "run" which performs the executing of the software, plus the following listed modules.

- \* calsplib.f     Main program
- \* splib.f             Includes all the subroutines used in the underlying BEM code.
- \* pfield.f           Includes subroutine "pfield" which is used to calculate the displacement field and traction field at nodes. It can be replaced by a user defined incident wave.

### ***PART III USING THE LIBRARY***

After getting everything set on the computer, a user can follow the steps below to run the program for a particular task. (paragraphs which are in capital form are messages which will be on screen when the program is running)

*Step (1)* Type run

There will be a message and prompt on the screen as:

```
WELCOME TO THE ELASTIC WAVE ANALYSIS SPHEROID LIBRARY  
THE LIBRARY HAS BEEN SET TO RUN FOR SCATTERING FROM A SPHEROID  
  
PLEASE TYPE IN THE KT # AT WHICH YOU WANT TO RUN THE PROGRAM  
(TYPE A SINGLE DIGIT NUMBER)
```

Then there will be the following prompt:

```
PLEASE SPECIFY THE GEOMETRY PARAMETERS OF THE SPHEROID  
TYPE IN PARAMETERS FOR X Y Z DIRECTIONS  
(TYPE THREE DIGITS SEPARATED BY TWO COMMAS )  
(e.g. 1,1,1 FOR SPHERE, OR 3,3,1 FOR A 3:3:1 SPHEROID)
```

Then there will be the following message:

```
READING IN THE MATRIX FROM LIBRARY, PLEASE WAIT FOR A MOMENT.
```

The code is reading in a matrix from the matrix data file, it may take a couple of minutes.

Then a user will be asked the following question:

```
MORE THAN 1 INCIDENT WAVE?
```

(TYPE IN y IF ANSWER IS YES, n IF ANSWER IS NO)

which means whether or not more than one incident wave case needs to be computed at one time. If y, follow step (2a), If n, follow step(2b).

*Step (2a)* The following prompt will appear:

PLEASE TYPE IN THE TOTAL NUMBER OF INCIDENT WAVES

(A SINGLE OR DOUBLE DIGIT NUMBER)

Then there will be the following prompt:

YOU ASKED TO CALCULATE\_\_\_\_\_ INCIDENT WAVES.

NOW, FOR THE NO.\_\_\_\_INCIDENT WAVE

PLEASE SPECIFY THE TYPE OF WAVE

( p IF P-WAVE, s IF S-WAVE)

then follow step (3p) for p-wave, step (3s) for s-wave.

*Step (2b)* The following message will appear:

PLEASE SPECIFY THE TYPE OF WAVE ( p if P-WAVE, s if S-WAVE)

then follow step (3p) for p-wave, step (3s) for s-wave.

*Step (3p)* The user will need to enter the incident angles THETA and PHI. The definition of incident angles and polarization unit vector are defined in Figure 1b. The following prompt will appear:

YOU ARE USING A P-WAVE, PLEASE TYPE IN THETA AND PHI  
 (THETA--ANGLE BETWEEN THE INCIDENT WAVE AND X3 AXIS)  
 (PHI--ANGLE BETWEEN THE PROJECTION OF INCIDENT WAVE IN X1-X2 PLANE  
 AND X1 AXIS)  
 (TYPE TWO REAL NUMBERS SEPARATED BY A COMMA)

*Step (3s)* The user will be asked to type in incident angle THETA, PHI and ALPHA:

YOU ARE USING A S-WAVE, PLEASE TYPE IN THETA,PHI,ALPHA  
 (THETA--ANGLE BETWEEN THE INCIDENT WAVE AND X3 AXIS)  
 (PHI--ANGLE BETWEEN THE PROJECTION OF INCIDENT WAVE IN X1-X2 PLANE  
 AND X1 AXIS)  
 (ALPHA--POLARIZATION ANGLE FOR SHEAR WAVE)  
 (TYPE THREE REAL NUMBERS SEPARATED BY TWO COMMAS)

The next prompt will be:

READY TO GET BOUNDARY QUANTITIES AT NODES !

(TYPE go IF YOU WANT TO CONTINUE, OTHERWISE TYPE no TO STOP)

If go, the next prompt will appear:

(If no, the program will stop and be ready to run again)

FOR THE WAVENUMBER,  $K_T =$  \_\_\_\_\_  $K_L =$

THE BOUNDARY VALUES OF DISPLACEMENT HAVE NOW BEEN DETERMINED.

(THESE COULD BE PRINTED LATER IF DESIRED)

RESULT FROM AULD INTEGRATION IS \_\_\_\_\_ .

Then the user will get the following prompt:

ARE YOU INTERESTED IN BACKSCATTERED AND SPECULAR SCATTERED  
AMPLITUDE ONLY?

OR, ARE YOU INTERESTED IN OTHER DIRECTIONS AS WELL?

(TYPE a FOR BS AND SS ONLY, TYPE b FOR OTHER DIRECTIONS)

Then proceed to step (4a) or (4b) accordingly.

*Step (4a)* The following message will appear:

IS FARFIELD SUFFICIENT, IF SO TYPE IN 1000

IF NEARFIELD (SMALLER R) IS DESIRED, TYPE IN DESIRED NEARFIELD R

The farfield scattering amplitudes (or equivalent scattering amplitudes for nearfield), which include the P-wave, Stheta-wave and Sphi-wave amplitudes will be presented on the screen. Plots of farfield scattering amplitude at PHI incident as a function of THETA will appear for all three waves if only one incident wave was chosen initially. Otherwise, the plots will appear only for the last wave chosen.

Now follow step (5).

*Step (4b)* The following message will appear:

TYPE IN NUMBER OF POINTS DESIRED (WHOLE NUMBER)

Then there will be the following message on screen:

FOR POINT 1, TYPE IN DESIRED R, THETA, PHI

( THREE REAL NUMBERS SEPARATED BY 2 COMMAS)

FOR POINT 2, TYPE IN DESIRED R, THETA, PHI

( THREE REAL NUMBERS SEPARATED BY 2 COMMAS)

:

:

The equivalent scattering amplitudes , which include the P-wave, Stheta-wave and Sphi-wave equivalent amplitudes will be presented on the screen. Plots of farfield scattering amplitude at PHI incident as a function of THETA will appear for all three waves if only one incident wave was chosen initially. Otherwise, the plots will appear only for the last wave chosen.

Now follow step (5).

amplitudes for those desired points will be presented on the screen.

Then follow step (5).

*Step (5)* If more than 1 incident case needs to be evaluated, there will be the following

message:

\*\*\*\*\*FINISH COMPUTING FOR NO 1 INCIDENT WAVE\*\*\*\*\*

YOU ASKED TO CALCULATE \_\_\_\_\_INCIDENT WAVES.

NOW, FOR THE NO.\_\_\_\_INCIDENT WAVE

PLEASE SPECIFY THE TYPE OF WAVE

( p IF P-WAVE, s IF S-WAVE)

Then go back to step (3p) or (3s). The processes from step (3p) or (3s) to step (5) will need to be repeated for each incident wave.

### ***PART IV EXAMPLE / DEMONSTRATION***

Suppose we are interested in the backscattered amplitude by a 3:3:1 spheroid when impinged by a unit P-Wave in x3 direction, the following steps are what a user needs to do:

(1) Type run

(2) Type 1

for  $k_1 a$

(3) Type 3,3,1

for the geometry parameter for x,y,z direction.

(4) Type n

only one incident wave

(5) Type p

represents p-wave

(6) Type 0,0

THETA=0 degree, PHI=0 degree

(7) Type go

let the program do the calculations

(8) Type a

backscattered and specular scattered scattering amplitudes are desired.

(9) Type 1000

farfield is sufficient.

Note:

- 1) The answers you type are case sensitive, all commands typed should be in lower case.
- 2) You can always press Ctrl and C key at same time to kill the process. Start it again by typing run.

### *References*

1. P.J. Schafbuch, Application of the boundary element method to elastic wave scattering problems in ultrasonic nondestructive evaluation, PhD Dissertation, Iowa State University, 1991.

Figure 1a General scattering problem: Defect in fields ( reproduced from [1] )

Figure 1b General scattering problem: Wave and polarization unit vector definitions

(reproduced from [1] )

Figure 2a

Figure 2b

Figure 3a

Figure 3b

## APPENDIX A ELASTIC WAVE ANALYSIS SPHEROID (EWAS)

LIBRARY .....	128
USER'S MANUAL.....	128
PART I    GENERAL INFORMATION	
ABOUT EWAS LIBRARY .....	128
PART II    SOFTWARE INSTALLATION .....	129
PART III    USING THE LIBRARY .....	130
PART IV    EXAMPLE / DEMONSTRATION..	137
Figure 1 a .....	139
Figure 2a .....	141

## APPENDIX B

### COEFFICIENT MATRICES FOR COMPOSITE UNIT CELL

#### B.1. Entire-Cell Model

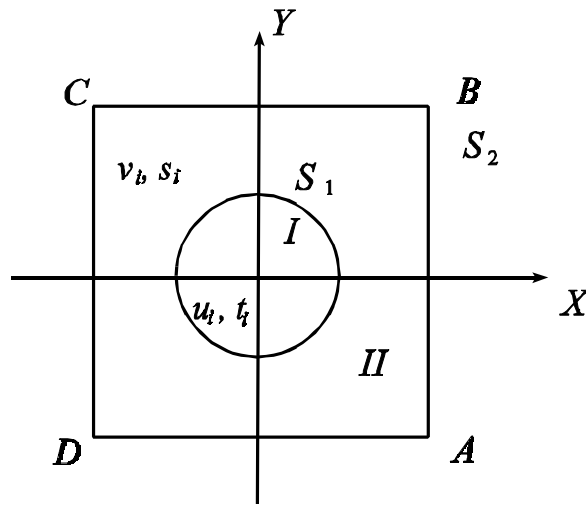


Figure B-1 Composite entire-cell model

For an entire-cell model as in Fig. B-1, if there are  $N_1$  Nodes on  $S_1$ ,  $N_2$  nodes on  $S_2$ .

The BIE for the matrix material  $II$  is eqn. (5) in Chapter 2(repeated here).

$$c_{ji}(p)v_i(p) = \int_{S_1+S_2} [v_i(q)T_{ij}(p,q) - s_i(q)U_{ij}(p,q)]ds(q). \quad (5)$$

Notice that boundary conditions eqn(1) in Chapter 2 on  $BC$  and  $AD$  actually involve one unknown  $C$ , the additional eqn(2) in Chapter 2 (repeated here),

$$\int_{BC} \mathbf{s}_y(x, a) dx = 0 \quad (2)$$

is needed,

Hence, there are in total  $2*(N_1+N_2)+1$  equations for the matrix material. The corresponding discretized equations in matrix form is as follows:

$$\begin{bmatrix} \mathbf{A}_1^{II} & \mathbf{A}_2^{II} & \mathbf{A}_3^{II} & \mathbf{A}_4^{II} \\ \mathbf{0} & \mathbf{a}_1 & \mathbf{0} & \mathbf{a}_2 \end{bmatrix} \begin{Bmatrix} \mathbf{v}(S_1) \\ \mathbf{vs}(S_2) \\ \mathbf{s}(S_1) \\ C \end{Bmatrix} = \begin{Bmatrix} \mathbf{BTT2} \\ 0 \end{Bmatrix}, \quad (B.1)$$

where  $\mathbf{v}(S_1)$  is the displacement vector for nodes on  $S_1$  on the matrix side, the bold form is used here to indicate vector/Matrix. The superscript  $II$  represents material  $II$  (the matrix material). Similarly,  $\mathbf{vs}(S_2)$  represents the unknowns for nodes on  $S_2$ ,  $\mathbf{s}(S_1)$  is the traction vector for nodes on  $S_1$  on the matrix side,  $C$  is the unknown constant in boundary condition eqn. (1) in Chapter 2.  $\mathbf{BTT2}$  is the corresponding right hand side known vector for this set of BIEs.

The first row in eqn. (B.1) represents the discretized BIEs for the matrix material, while the second is the discretized form of the additional eqn. (2) in Chapter 2.

For the fiber material, the BIE is eqn. (4) in Chapter 2 (repeated here)

$$c_{ji}(p)u_i(p) = \int_{S_1} [u_i(q)T_{ij}(p, q) - t_i(q)U_{ij}(p, q)] ds(q). \quad (4)$$

The discretized form is

$$[\mathbf{A}_1^T \quad \mathbf{A}_2^T] \begin{Bmatrix} \mathbf{u}(S_1) \\ \mathbf{t}(S_1) \end{Bmatrix} = \{\mathbf{0}\} \quad (\text{B.2})$$

where  $\mathbf{u}(S_1)$  is the displacement vector for nodes on  $S_1$  on the fiber side,  $\mathbf{t}(S_1)$  is the traction vector for nodes on  $S_1$  on the fiber side. There are  $2*N_1$  equations in Eqn(B.2).

The interface condition for nodal points on  $S_1$  are eqn. (14) and eqn. (15) in Chapter 2 (repeated here) depending on whether overlap occurs,

$$\begin{Bmatrix} v_x - u_x \\ v_y - u_y \end{Bmatrix} = [T]^{-1} \begin{bmatrix} M_s & \\ & M_n \end{bmatrix} [T] \begin{Bmatrix} t_x \\ t_y \end{Bmatrix} \quad (14)$$

when  $t_n > 0$ , *i.e.*  $v_n - u_n > 0$ .

$$\begin{Bmatrix} v_x - u_x \\ v_y - u_y \end{Bmatrix} = [T]^{-1} \begin{bmatrix} M_s & \\ & 0 \end{bmatrix} [T] \begin{Bmatrix} t_x \\ t_y \end{Bmatrix} \quad (15)$$

when  $t_n \leq 0$ , *i.e.*  $v_n - u_n \leq 0$ .

Further, the interface condition for nodal point on  $S_1$  can be written in a single form for the above two cases and also for a disbonding interface, if a new matrix  $\mathbf{B}$  is introduced.

Let the interface condition be written as

$$\begin{Bmatrix} v_x - u_x \\ v_y - u_y \end{Bmatrix} = \begin{bmatrix} B_{11} & B_{12} \\ B_{21} & B_{22} \end{bmatrix} \begin{Bmatrix} t_x \\ t_y \end{Bmatrix}. \quad (\text{B.3})$$

It can be seen that at a normal interface where  $t_n > 0$ ,

$$\begin{aligned} B_{11} &= M_s \sin^2 \mathbf{a} + M_n \cos^2 \mathbf{a} \\ B_{12} &= B_{21} = -M_s \sin \mathbf{a} \cos \mathbf{a} + M_n \sin \mathbf{a} \cos \mathbf{a} \\ B_{22} &= M_s \cos^2 \mathbf{a} + M_n \sin^2 \mathbf{a}. \end{aligned} \quad (\text{B.4})$$

At nodes where overlap occurs, *i.e.*  $t_n \leq 0$ ,

$$\begin{aligned}
B_{11} &= M_s \sin^2 \mathbf{a} \\
B_{12} &= B_{21} = -M_s \sin \mathbf{a} \cos \mathbf{a} \\
B_{22} &= M_s \cos^2 \mathbf{a} .
\end{aligned} \tag{B.5}$$

At nodes where disbonding take place

$$\begin{aligned}
B_{11} &= \text{HUGE} \\
B_{12} &= B_{21} = 0 \\
B_{22} &= \text{HUGE}
\end{aligned} \tag{B.6}$$

where HUGE is a big number.

Notice also the traction interface conditions,

$$\begin{Bmatrix} t_x + s_x \\ t_y + s_y \end{Bmatrix} = \{\mathbf{0}\} , \tag{B.7}$$

the coupled equation for the full model can be arranged as

$$\begin{bmatrix} \mathbf{A}_1'' & \mathbf{A}_2'' & \mathbf{A}_3'' & \mathbf{0} & \mathbf{A}_4'' \\ \mathbf{0} & \mathbf{0} & -\mathbf{A}_2^I & \mathbf{A}_1^I & \mathbf{0} \\ \mathbf{I} & \mathbf{0} & \mathbf{B} & -\mathbf{I} & \mathbf{0} \\ \mathbf{0} & \mathbf{a}_1 & \mathbf{0} & \mathbf{0} & \mathbf{a}_2 \end{bmatrix} \begin{Bmatrix} \mathbf{v}(S_1) \\ \mathbf{v}(S_2) \\ \mathbf{s}(S_1) \\ \mathbf{u}(S_1) \\ C \end{Bmatrix} = \begin{Bmatrix} \mathbf{BTT2} \\ \mathbf{0} \\ \mathbf{0} \\ \mathbf{0} \end{Bmatrix} . \tag{B.8}$$

where  $\mathbf{I}$  is the identity matrix. Eqn (B.5) contains  $2*N_2+6*N_1+1$  unknowns and the same number of equations.

## ***B.2. One-Quadrant Model***

For the 1/4 Model as in Fig. B-2, let  $S_1 = DO \cup OE$ ,  $S_2 = ED$ ,  $S_3 = AB \cup BC \cup CE$

the BIE for the fiber can be written as

$$c_{ji}(p)u_i(p) = \int_{S_1+S_2} [u_i(q)T_{ij}(p,q) - t_i(q)U_{ij}(p,q)]ds(q) \tag{B.9}$$

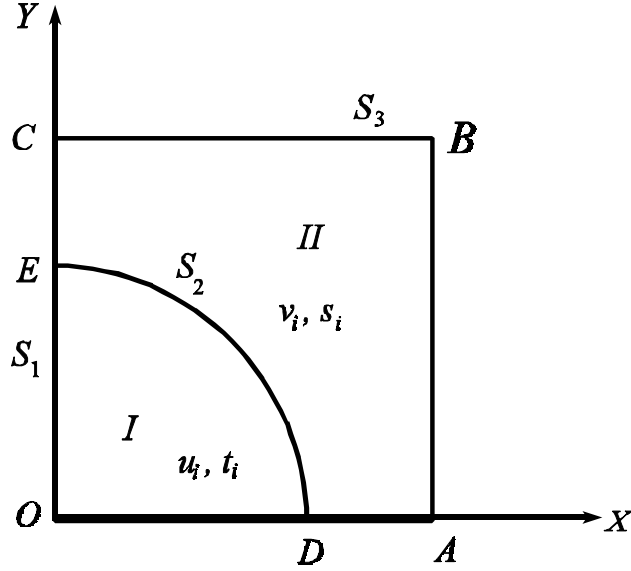


Figure B.2 one-quadrant model

The following discretized BIE can be obtained:

$$\begin{bmatrix} \mathbf{A}_1^I & \mathbf{A}_2^I & \mathbf{A}_3^I \end{bmatrix} \begin{Bmatrix} \mathbf{u}(S_1) \\ \mathbf{u}(S_2) \\ \mathbf{t}(S_2) \end{Bmatrix} = \{\mathbf{BTT1}\}, \quad (\text{B.10})$$

again, superscript  $I$  indicates material  $I$ .

For the matrix material, the BIE is:

$$c_{ji}(p)v_i(p) = \int_{S_2+S_3} [v_i(q)T_{ij}(p,q) - s_i(q)U_{ij}(p,q)]ds(q). \quad (\text{B.11})$$

The boundary condition for a quarter model for determining Young's modulus is similar to that for the entire-cell model except at two special points, namely  $D$  and  $E$  which are both corner point as well as interface point. The boundary condition is ( $D, E$  exclusive):

$$\begin{aligned}
u_x = 1 \quad t_y = 0 & \quad \text{on } AB \\
t_x = 0 \quad u_y = -C & \quad \text{on } BC \\
u_x = 0 \quad t_y = 0 & \quad \text{on } CO \\
t_x = 0 \quad u_y = 0 & \quad \text{on } OA
\end{aligned} \tag{B.12}$$

Consider the boundary condition at  $D$  and  $E$ . It has been noticed by researchers on BEM that for such points, special attention is needed [1]. For example, at the special points  $E$ , let  $E_I$  denotes node  $E$  on the fiber side, and  $E_{II}$  denotes node  $E$  on the matrix side as in Figure B-3.

There are twelve unknowns at  $E_I$  and  $E_{II}$ . They are:

$$\begin{aligned}
u_x(E_I), \quad u_y(E_I), \quad t_x^1(E_I), \quad t_y^1(E_I), \quad t_x^2(E_I), \quad t_y^2(E_I) \\
v_x(E_{II}), \quad v_y(E_{II}), \quad s_x^3(E_{II}), \quad s_y^3(E_{II}), \quad s_x^4(E_{II}), \quad s_y^4(E_{II})
\end{aligned}$$

where superscripts 1, 2, 3, 4 are used to indicate the segment numbers which are the same as the numbers in circles in Fig. B-3. There are also twelve equations at such points  $E_I$  and  $E_{II}$ . They are:

1. boundary conditions at  $E_I$  and  $E_{II}$ .

$$u_x(E_I) = 0, \quad v_x(E_{II}) = 0, \quad t_y^1(E_I) = 0, \quad s_y^4(E_{II}) = 0. \tag{B.13}$$

2. shear equality

$$t_x^2(E_I) = 0, \quad s_x^3(E_{II}) = 0. \tag{B.14}$$

3. interface condition

$$\begin{aligned}
t_y^2(E_I) &= -s_y^3(E_{II}) \\
v_y(E_{II}) - u_y(E_I) &= B_{22}t_y^2(E_I).
\end{aligned} \tag{B.15}$$

collocations at  $E_I$  and  $E_{II}$  gives four equations. Hence, there is just right number of equations to determine all the unknowns at the corner-interface point. Similarly, the same is true for  $D$ .

In the implementation, both  $D$  and  $E$  are considered as interface points which have eight unknowns at each point. At  $E$ , they are:

$$\begin{aligned} u_x(E_I), \quad u_y(E_I), \quad t_x^1(E_I), \quad t_y^2(E_I), \\ v_x(E_{II}), \quad v_y(E_{II}), \quad s_y^3(E_{II}), \quad s_x^4(E_{II}). \end{aligned}$$

The other four unknowns at  $E$  are specified as boundary conditions, i.e.

$$\begin{aligned} t_y^1(E_I) = t_x^2(E_I) = 0, \\ s_x^3(E_{II}) = s_y^4(E_{II}) = 0. \end{aligned} \tag{B.16}$$

By this arrangement, the traction discontinuity across the interface at  $E$  can be captured, i.e.  $t_x^1(E_I) \neq s_x^4(E_{II})$ . This traction discontinuity has been observed when fiber and matrix are different materials.

In the code, the four interface conditions for  $E$  are

$$\begin{aligned} u_x(E_I) &= v_x(E_{II}) \\ v_y(E_{II}) - u_y(E_I) &= B_{22}t_y^2(E_I) \\ u_x(E_I) &= 0 \\ t_y^2(E_I) &= -s_y^3(E_{II}). \end{aligned} \tag{B.17}$$

Similarly, at  $D$ , the eight unknowns are

$$\begin{aligned}
 &u_x(D_I), \quad u_y(D_I), \quad t_y^5(D_I), \quad t_x^6(D_I), \\
 &v_x(D_{II}), \quad v_y(D_{II}), \quad s_x^7(D_{II}), \quad s_y^8(D_{II}).
 \end{aligned}
 \tag{B.18}$$

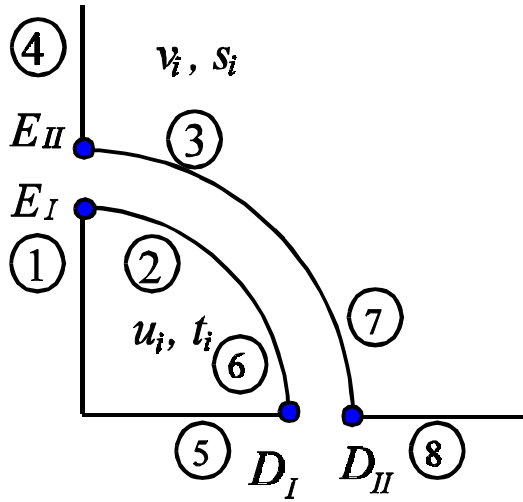


Figure B-3 corner-interface point

The boundary conditions are

$$\begin{aligned}
 t_x^5(D_I) &= t_y^6(D_I) = 0, \\
 s_x^8(D_{II}) &= s_y^7(D_{II}) = 0.
 \end{aligned}
 \tag{B.19}$$

The interface conditions are given as

$$\begin{aligned}
 v_x(D_{II}) - u_x(D_I) &= B_{11}t_x^6(D_I), \\
 u_y(D_I) &= v_y(D_{II}), \\
 t_x^6(D_I) &= -s_x^7(D_{II}), \\
 u_y(D_I) &= 0.
 \end{aligned}
 \tag{B.20}$$

Again, notice that the boundary conditions on BC involve an unknown  $C$ . Thus an additional equation, (same as eqn (2)) is needed.

$$\int_{BC} \mathbf{s}_y(x, a) dx = 0. \quad (2)$$

The discretized form can be arranged as:

$$\begin{bmatrix} \mathbf{A}_1'' & \mathbf{A}_2'' & \mathbf{A}_3'' & \mathbf{A}_4'' \\ \mathbf{0} & \mathbf{a}_1 & \mathbf{0} & \mathbf{a}_2 \end{bmatrix} \begin{Bmatrix} \mathbf{v}(S_2) \\ \mathbf{vs}(S_3) \\ \mathbf{s}(S_2) \\ C \end{Bmatrix} = \begin{Bmatrix} \mathbf{BTT2} \\ 0 \end{Bmatrix}. \quad (\text{B.21})$$

The interface condition at any interface points beside  $D$  and  $E$  are the same as for the entire-cell model, namely, eqns (B.3--B.7). The final system of equations for the 1/4 model can be arranged as:

$$\begin{bmatrix} \mathbf{A}_1' & \mathbf{A}_2' & \mathbf{0} & \mathbf{A}_3' & \mathbf{0} & \mathbf{0} & \mathbf{A}_4' \\ \mathbf{0} & \mathbf{0} & \mathbf{A}_2'' & \mathbf{0} & \mathbf{A}_1'' & \mathbf{A}_3'' & \mathbf{0} \\ \mathbf{0} & -\mathbf{I} & \mathbf{0} & -\mathbf{B} & \mathbf{I} & \mathbf{0} & \mathbf{0} \\ \mathbf{0} & \mathbf{0} & \mathbf{a}_1 & \mathbf{0} & \mathbf{0} & \mathbf{0} & \mathbf{a}_2 \end{bmatrix} \begin{Bmatrix} \mathbf{ut}(S_1) \\ \mathbf{u}(S_2) \\ \mathbf{vs}(S_3) \\ \mathbf{t}(S_2) \\ \mathbf{v}(S_2) \\ \mathbf{s}(S_2) \\ C \end{Bmatrix} = \begin{Bmatrix} \mathbf{BTT1} \\ \mathbf{BTT2} \\ \mathbf{0} \\ 0 \end{Bmatrix}. \quad (\text{B.22})$$

### *References*

1. M. Chati, Prediction of the elastic properties of unidirectional fiber reinforced composites, Master thesis, Iowa State University, 1995.

## **ACKNOWLEDGMENTS**

First and foremost I would like to express my most sincere thanks to my advisor, Dr. Frank J. Rizzo for leading me into the interesting field of boundary element analysis, and for his continuous guidance, patience and encouragement during my study. His contributions to my education have gone far beyond academics, and for that I will always be grateful.

I thank Professors. J.E. Bernard, T.J. Rudolphi, R.A. Roberts, P.E. Sacks, D.O. Adams for being willing to serve on my Program of Study committee and to readily provide assistance and direction whenever needed. I also thank Professor Paul Martin of the Department of Mathematics, University of Manchester, for his contributions to many parts of this research. Special thanks go to professor R.A. Roberts for many helpful discussions on wave topics and for providing the code for numerical implementing the halfspace Green's function, which makes a major part of the research in this thesis possible. I also want to thank faculty members in AEEM department who have frequently and freely offered up their knowledge and help , especially D.E. Chimenti, L.W. Schmerr, A.K. Mitra, and T.R. Rogge.

I thank Prof. Y. Liu of University of Cincinnati and Dr. D. Zhang of Optimal Analysis, Inc. for their willingness to offer their expertise on BEM from the day I started working in this area. Special thanks go to Dr. D. Zhang for numerous discussions on my research.

Portions of this work have been supported by the National Science Foundation and the National Institute of Standards and Technology with the cooperation of the Colorado School of Mines under contract # 4-41578 and also by the National Institute for Standards and Technology, Gaithersburg, MD, under grand No. 60NANB6D0210.

Thanks are also due the AEEM Department, Center for nondestructive Evaluation and College of Engineering of Iowa State University for additional support.

Last but not least, my thanks go to my parents, my husband Wen and my daughter Feifei, for their sacrifice, patience and support during the course of achieving this goal. I dedicate this dissertation to my family.

## VITA

**NAME OF AUTHOR:** Lingyun Pan

**DATE AND PLACE OF BIRTH:** January 15, 1966, Yixin, Jiangsu, P.R.China

**DEGREE AWARDED:**

**Ph. D** Engineering Mechanics, Iowa State University, 1997.

**M.S.** Computational Mechanics, Nanjing Aeronautical Institute, China, 1988.

**B.S.** High Altitude Aircraft Equipment, Nanjing Aeronautical Institute, 1985.

**AWARDS AND AFFILIATIONS:**

Member of Sigma Xi, Tau Beta Pi, Phi Kappa Phi.

Member of Society for Women in Engineering.

Member of A.S.M.E. .

**PROFESSIONAL EXPERIENCE:**

Lecturer, Department of Aerospace Engineering, Nanjing Aerospace Institute, 1988-1993.

Research and Teaching Assistant, Department of Aerospace Engineering and Engineering Mechanics, Iowa State University, 1993-1997.

**PROFESSIONAL PUBLICATIONS:**

L. Pan, and F.J. Rizzo, "Some Efficient Boundary Integral Strategies for Wave Problems in an Elastodynamic Halfspace.", submitted to Computer Methods in Applied Mechanics and Engineering.

L. Pan, D.O. Adams and F.J. Rizzo, "BEM Analysis for Composite Materials with a Library of Green's Functions", will be published in Computer & Structures.

L. Pan and F.J. Rizzo, "Discretized Green's Functions and an Idea for a Library", 24th Midwest Mechanics Conference, Ames, IA, Oct. 2-5, 1995.

L. Pan, H. Gu and Xihong Din, "A Hybrid Three-Dimensional Super element for Composite Structures", On 2nd Conference of China Composite Community, Journal of Nanjing Aeronautical Institute, Vol. 24, No. 5, Oct. 1992, pp. 632-639.

## APPENDIX B COEFFICIENT MATRICES FOR COMPOSITE

UNIT CELL.....	146
B.1. Entire-Cell Model.....	146
B.2. One-Quadrant Model.....	149
Reference.....	154
ACKNOWLEDGMENTS.....	155